pp 757–795. © Royal Aeronautical Society 2016
doi: 10.1017/aer.2016.30

Numerical and experimental validation of a morphed wing geometry using Price-Païdoussis wind-tunnel testing*

A. Koreanschi, O. Sugar-Gabor and R.M. Botez
ruxandra@gpa.etsmtl.ca
Laboratory of Applied Research in Active Controls
Avionics and AeroServoElasticity LARCASE
École de technologie supérieure ETS
University of Quebec, Montreal, Quebec
Canada

ABSTRACT

An experimental validation of an optimised wing geometry in the Price-Païdoussis subsonic wind tunnel is presented. Two wing models were manufactured using optimised glass fibre composite and tested at three speeds and various angle-of-attack. These wing models were constructed based on the original aerofoil shape of the ATR 42 aircraft and an optimised version of the same aerofoil for a flight condition of Mach number equal to 0.1 and angle-of-attack of 0°. The aerofoil's optimisation was realised using an 'in-house' genetic algorithm coupled with a cubic spline reconstruction routine, and was analysed using XFoil aerodynamic solver. The optimisation was concentrated on improving the laminar flow on the upper surface of the wing, between 10% and 70% of the chord. XFoil-predicted pressure distributions were compared with experimental data obtained in the wind tunnel. The transition position was estimated from the experimental pressure data using a second derivative methodology and was compared with the transition predicted by XFoil code. The results have shown the agreement between numerical and experimental data. The wind-tunnel tests have shown that the improvement of the laminar flow of the optimised wing is higher than the value predicted numerically.

Keywords: Aerodynamics; XFoil; transition flow; morphing wing; wind-tunnel tests; genetic algorithms; optimisation

* The authors' names were originally presented in the wrong order. A notice detailing this has been published and the error rectified in the online PDF and HTML copies.

Received 25 April 2015; revised 15 September 2015; accepted 18 November 2015.

NOMENCLATURE

A_f	attraction factor
E_1	longitudinal elastic modulus
E_2	transversal elastic modulus
C_d	drag coefficient
C_l	lift coefficient
Cp	pressure coefficient
F_f	fitness function
G_{12}	longitudinal shear strength
H	wind tunnel height
L	wind tunnel length
μ	dynamic viscosity
M	mach number
P	pressure
P_s	probability of selection function
S_{1T}	longitudinal tension strength
S_{2T}	transversal tension strength
S_{1C}	longitudinal compression strength
S_{2C}	transversal compression strength
Up_{Tr}	upper surface transition
u	x direction speed component
v	y direction speed component
w	z direction speed component
W	wind tunnel width
x	probability of selection function parameter
y	probability of selection function parameter
z	probability of selection function parameter

Abbreviations

2D	bidimensional
CRIAQ	Consortium de Recherche et Innovation en Aerospatiale du Quebec
ETS	Ecole de Technologie Superieure
GARDN	Green Aviation Research & Developement Network
LARCASE	Aeronautical Research Laboratory in Active Control, Avionics and Aeroservoelasticity
NRC	National Research Center
PID	Proportional Integral Derivative
PTA	Pressure Transducer Array
SMA	Shape Memory Alloy
UAV	Unmanned Aerial Vehicle
UD/1D	Uni-dimensional

1.0 INTRODUCTION

In the context of a world in continuous change, the aerospace industry has to develop greener and more efficient aircraft, which consume less fuel and have a smaller CO_2 footprint. The

https://doi.org/10.1017/aer.2016.30 Published online by Cambridge University Press

aerospace industry has therefore developed methods to improve the aerodynamical properties of aircraft. A number of international collaborations and projects were established to tackle this problem.

One research direction regards the development of new methods for flight trajectories optimisation. Several methods are underway at various academic laboratories, mostly in collaboration with industrial partners. One such collaboration took place between the teams in the LARCASE laboratory and CMC Electronics-Esterline in the GARDN project. The main objective of the collaboration was to optimise the vertical and horizontal path of the aircraft within the Flight Management System by taking into account the Required Time of Arrival, the wind grids and meteorological conditions. The main motivation of the project was to reduce overall carbon emissions and flight costs. This project was funded by the Green Aviation Research Development Business Led Network GARDN in its second round[1,2].

Another research direction regards the optimisation of the aircraft itself, which can be achieved by modifying any or all of its parts: wing, fuselage, nose, tail, etc. The most common area, and the one with the greatest impact, is the aircraft wing. There are several ways in which a wing can be modified: in-plane modifications, which can be done by optimising the span or chord for example, out-of-plane modifications, which refers to modifying the twist and bending of the wing, and optimisation of the aerofoil or aerofoils that compose the wing. Also, adaptive, morphing wings can be effectively used to replace conventional high-lift devices[3,4], or the conventional control surfaces[5].

In-plane and out-of-plane wing modifications are radical types of optimisation that require complete reconstruction of the wing and, thus, cannot be introduced directly onto an existing aircraft due to certification considerations and high costs. In addition, their aerodynamic properties were not completely demonstrated, with the exception of projects dedicated to UAV developments. Gamboa et al[6] designed an UAV wing capable of independent span and chord changes, using a telescopic spar and a rib system. The numerical analysis demonstrated drag reductions of up to 23% when compared to the non-morphing geometry. Falcão et al[7] designed and tested a morphing winglet for a military UAV, achieving important performance improvement by simply changing the winglet cant and toe angles. Another research on UAV wing morphing was done by Sugar Gabor et al[8,9], where the upper-surface of the wing was optimised between the leading edge and 55% of the chord and they also explored morphing of the full wing's geometry.

For further references on these types of optimisation, Sofla et al[10] and Vasista et al[11] have presented an exhaustive state-of-the-art list of wing geometry modifications.

'Aerofoil optimisation' is a much more accessible method of modifying wing geometry. It is a branch of the wing modification domain that has been well studied, as attested by the large number of different aerofoils that represent compromises to obtain specific performance levels. The aerofoil geometry (e.g. symmetric shape, more cambered aerofoil, thicker aerofoil) was manipulated to improve its performances for subsonic, transonic or supersonic flight or across a range of speeds passing from one regime to another[12,13].

The purpose of the 'in-flight modification' of the aerofoil shape was to enable the aircraft to improve its wing parameters as a function of the flight conditions in which it flies (speed, global or local angle-of-attack, aileron deflection, flap deflection, etc.). This approach enables the aircraft to extend its flight envelope and to become more flexible during flight without having to change its wing shape radically. The climbing and descending phases of the flight are two practical situations in which the optimisation of the wing shape can improve the performances of the aircraft and could also lead to further improvements in the design of the landing gear. Another practical situation would be the minimisation of the shock wave or

https://doi.org/10.1017/aer.2016.30 Published online by Cambridge University Press

'buffet' on the wing for the transonic flight regime by modifications to the upper surface of the wing. The minimisation of the shockwave could lead to important reductions in drag.

Several experiments were conducted in the area of 'active aerofoil optimisation'. One of the most recent experiments was performed in the CRIAQ 7.1 project, in which collaboration took place between aerospace industrial teams at Bombardier and Thales, and academic partners from the École de Téchnologie Supérieure (ETS) and École Polytéchnique, and the National Aerospace Research Center (NRC). The purpose of the project was to demonstrate the capabilities of morphing wings for developing the flow transition from laminar to turbulent[14,15]. Morphing was achieved by replacing the upper surface of the wing between 7% and 70% of the wing chord with a flexible carbon-Kevlar composite and by morphing it using two SMA actuation lines to obtain an optimised shape for each flight condition studied in a wind tunnel[16]. The optimisation was done using a genetic algorithm method coupled with the aerodynamic solver XFoil. The wind-tunnel tests have proven that the concept of upper surface morphing was viable, controllable, and gave good results, confirming the delay of the transition from laminar to turbulent flow as well as a reduction of the drag coefficient[17]. PID[18] and neuro-fuzzy controllers[19] were tested to prove that the ability to control the shape of the morphing system to determine the delay of the transition. They gave excellent results in both open[20] and closed loops[21].

Based on the CRIAQ 7.1 experience, another project was developed at the LARCASE laboratory. Its purpose was to develop a wind-tunnel active morphing model using electrical actuators, optimised epoxy-glass fibre composite skin, a PID controller and an 'in-house' genetic algorithm coupled with the XFoil aerodynamic solver. Another goal of this project was to demonstrate the morphing-aerofoil concept on a different wing, and therefore with different lengths of morphing upper-surface skin (10%c to 70%c). In this project, the ATR 42 wing model was manufactured totally from composite, instead of a combination of an upper-surface composite and aluminium wing body.

The project described in the paragraph above was a multi-disciplinary project, in which aerodynamic optimisation and analysis, composite material optimisation and manufacturing and active control of the morphing structure work together to obtain an active morphing wing.

This project was developed in two phases. *The first phase of the project, presented in this paper*, concentrated on several aspects: development of the aerodynamic shape optimisation algorithm, optimisation of the composite material and the manufacturing of two rigid wing models. The rigid wing models were based on the original ATR-42 aerofoil and one optimised version of the same aerofoil at a specific flight condition (angle-of-attack 0° and speed 34.6 m/s). The two rigid wing models were designed and developed with the purpose of validating the optimisation algorithm and the wind-tunnel experimental set-up. In addition, another purpose was to determine the necessity of wind-tunnel corrections and to test the composite material in wind-tunnel conditions.

The second phase of the project, which is not described in the present paper, treated the design and development of the morphing mechanism, numerical optimisation results for multiple flight conditions, control of the morphing upper surface and wind-tunnel experimental results for the active morphing wing.

The present paper is concentrating on the presentation of the general aspects of the project for three of the disciplines involved (aerodynamic optimisation, manufacturing, experimental testing) and on the results that validate the aerodynamic optimisation for two aerofoil shapes (original and one optimised shape) and on the validation of the method of post-processing the experimental data for obtaining information that can be successfully compared with the numeric results.

https://doi.org/10.1017/aer.2016.30 Published online by Cambridge University Press

2.0 METHODOLOGY

2.1 Problem description

Aerofoil shape changing can refer to the whole aerofoil or to just one section of it; for example, the aerofoil's upper surface, aileron section or leading edge, etc. The geometric characteristics of an aerofoil are its coordinates, chord length, thickness and camber. Based on these, the wing aerofoil is also described by its aerodynamical parameters, such as lift, drag, aerodynamic moment and pressure coefficients, and the region where the flow passes from laminar to turbulent, also known as transition regime. The purpose of the optimisation depends on the flow conditions for which the wing will be deployed. For an aircraft, and implicitly for a wing, these conditions are related to flight manoeuvres: take-off, cruise, landing, stall, etc. For example, in a take-off configuration the purpose would be to increase the maximum lift while keeping the drag constant, while for landing the purpose would be to maintain the lift and increase the drag at the same time. In both cases, the results could lead to the development of an aircraft that can safely operate with a shorter take-off or landing strip.

For the ATR 42 wing aerofoil, the morphing region was situated on the upper surface of the aerofoil and the objective was to obtain delay of the transition onset with the purpose of reducing the drag coefficient.

2.2 Genetic algorithm general description

For the optimisation of the aerofoil, an 'in-house' genetic algorithm was developed and verified with the Monte Carlo method. The aerodynamic analysis was done using the XFoil aerodynamic solver; a brief description of this solver is given in Section 2.4.

The genetic algorithm is a meta-heuristic method of optimisation inspired from nature, which uses various characteristics of the object to be optimised as 'genes'. The genes were used to create new objects or individuals, based on the initial ones but having different characteristics. The creation of new individuals was done using two processes found in nature: 'cross-over' and 'mutation'. The cross-over is a process where the genes of two individuals are mixed in various proportions, usually equal, but more complicated functions can be used. The mutation process affects a percentage of the individuals resulted from the cross-over function(s), and changes the values of the genes using a percentage of mutation.

A fitness function was used to evaluate the optimisation level of the new individuals with respect to the original ones. This fitness function is a representation of the purpose of the optimisation and describes the ideal characteristics of the optimised individual.

The genetic algorithm method was well studied and validated in various problems; it uses different combinations of cross-over and mutation functions as well as problem-dependent fitness functions[22,23].

2.3 Application of the genetic algorithm to the aerofoil shape optimisation problem

This algorithm was applied in this paper to the geometric optimisation of the ATR 42 wing aerofoil upper surface.

In this project, the upper surface of the aerofoil was optimised between 10% and 70% of the chord, and no aileron was considered for the wing models. The length of the upper surface to be modified was chosen based on the fact that the leading edge part of a wing is manufactured separately for most civil aircraft, and thus from a morphing point of view it would be extremely difficult to introduce continuous modifications between a leading edge

https://doi.org/10.1017/aer.2016.30 Published online by Cambridge University Press

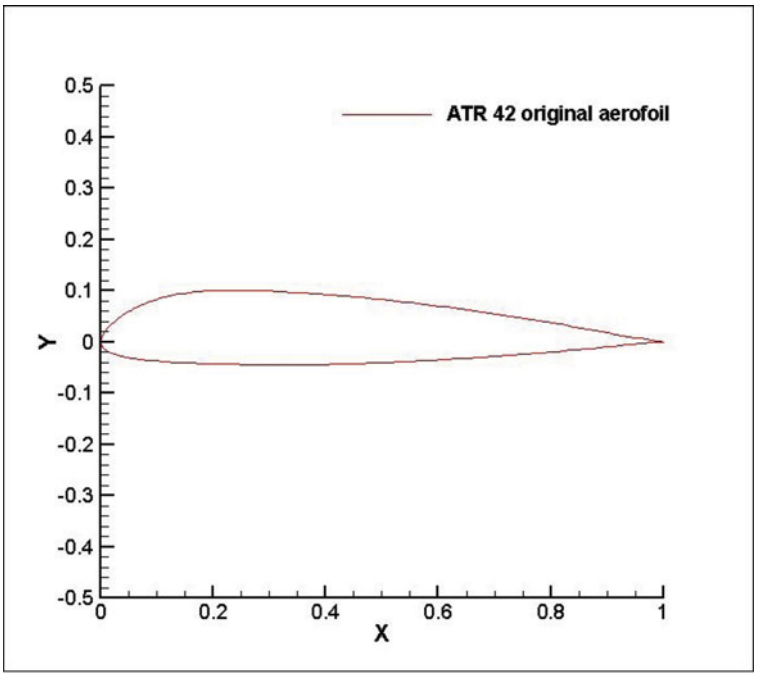

Figure 1. (Colour online) Shape of the ATR 42 wing aerofoil.

and the rest of the wing. The 70% end-limit was chosen because most aircraft have an aileron or flap starting near this point.

The area to be optimised was modified using two actuation points situated at 30% and 50% of the chord. Several other positions and number of actuators were tested: (a) one actuator situated at 30% of the chord; (b) one actuator situated at 50% of the chord; (c) two actuators situated at 30% and 50% of the chord; (d) two actuators situated at 25% and 40% of the chord; (e) three actuators situated at 20%, 35% and 50% of the chord and (f) four actuators situated at 20%, 35%, 45% and 60% of the chord. From all these combinations only version (c) has given the best results in terms of compromise between aerodynamic optimisation, structural forces need to push the skin, shape of the skin obtained after actuator deployment and coupled with the small space inside the wing box and actuator system design.

For the ATR 42 aerofoil, the optimisation objective was to obtain a reduction of the aerofoil's drag coefficient at constant angle-of-attack by delaying the position where the flow passes from laminar to turbulent, for small variations of speed and angle-of-attack. Because only small variations in speed were studied, only one optimised shape was considered for the first phase of the project and then analysed and tested over a range of angles of attack to observe its performances.

From the various geometrical characteristics that describe an aerofoil (the geometric characteristics of an aerofoil are its coordinates, chord length, thickness and camber), the authors have chosen to use the *coordinates of the actuation points as 'genes'*, thus reducing the number of unknowns to two – the two vertical displacements of the 'genes'. The upper surface of the aerofoil, between 10% and 70% of the chord, was reconstructed using ***cubic splines***, which proved to be a sufficiently accurate method[24].

https://doi.org/10.1017/aer.2016.30 Published online by Cambridge University Press

As mentioned before, for the aerofoil reconstruction of the upper surface cubic splines were used. The cubic splines give sufficient accuracy in reconstructing small curvatures. The spline functions are characterised by their shape on subintervals, between two control points. They are also known as *piece-wise polynomial real functions*. In interpolating problems, spline interpolation is often referred to as *polynomial interpolation*, due to the fact that it yields similar results; when using lower degree splines (e.g. bi-splines or cubic splines) the resulted curve is just as well traced as if interpolated with high-degree polynomials, but with the benefit of avoiding instability due to Runge's phenomenon.

The most-used spline interpolation is the cubic spline, which insures continuity up to, and including, the second-order derivatives, which allows the calculation of the curvature radius.

For the reconstruction of the aerofoil using cubic splines, the coordinates for the morphing skin which starts at 10%c and ends at 70%c and the 'genes' (actuation points), which are now defined as control points, were used.

As mentioned above, the optimisation method was coupled with the aerodynamic solver XFoil to calculate the aerodynamic characteristics of each new aerofoil that resulted from the optimisation process. The solver calculated the lift, drag, moment and pressure coefficients as well as the transition position based on the shape of the aerofoil and the flight conditions introduced. The methods employed by XFoil for the calculation of the aerodynamic parameters are presented in Section 2.4 of the Methodology. Given that the purpose of the optimisation was to reduce the drag coefficient by delaying the transition on the upper surface, the *fitness function, F_f,* was developed as a sum of multiple single-objective functions based on the aerodynamic parameters calculated with the XFoil solver:

$$F_f = w_1 \cdot C_l + w_2 \cdot \frac{1}{C_d} + w_3 \cdot Up_{Tr} + w_4 \cdot \frac{1}{Up_{Tr}} + w_5 \cdot \frac{C_l}{C_d} + w_6 \cdot \frac{Up_{Tr}}{C_d}, \qquad \ldots(1)$$

where w_i represent weights given by the user as natural numbers, positive or negative, depending on the purpose of the optimisation, U_{pTr} represents the transition point and F_f represents the *fitness function*.

The fitness function presented in Equation (1) is a multi-objective single-point optimisation function. Its purpose was to show that, by using all the aerodynamic characteristics provided by the XFoil analysis, and that, based on the particular objective of the optimisation, the fitness function used for the actual optimisation could be reduced to one of the functions presented in Equation (2).

Thus, in the particular case of optimising for drag coefficient reduction at constant angle-of-attack, the *fitness function F_f* was reduced to any of these expressions:

$$F_f = w_2 \cdot \frac{1}{C_d} \quad \text{or} \quad F_f = w_3 \cdot Up_{Tr} \quad \text{or} \quad F_f = w_6 \cdot \frac{Up_{Tr}}{C_d} \qquad \ldots(2)$$

Using either of the fitness functions presented in Equation (2), the optimisation results, in terms of the aerodynamic performances (lift and drag coefficient and upper surface transition) of the aerofoils, were similar.

In this genetic algorithm, the final value of the fitness function was not imposed, because the optimisation was considered free – no fixed value was associated to the objective, for example, there was no specific percentage of reduction that was demanded to be achieved – it was preferred to limit the number of generations and individuals. Based on convergence tests,

https://doi.org/10.1017/aer.2016.30 Published online by Cambridge University Press

20 generations and 40 individual aerofoils were considered sufficient, as changes in results were not obtained with higher values.

Because a maximum value for the fitness function was not imposed, a method for evaluating the performances of the aerofoils was developed based on the values of the fitness function the aerofoils obtained.

Thus, the maximum and minimum values of the fitness function were calculated for each generation. Then an interval was determined by using Equation (3):

$$\text{Interval} = \frac{\text{Fitness}_{\max} + \text{Fitness}_{\min}}{10} \quad \ldots(3)$$

Based on the fitness function values and the 'intervals', groups of fitness values were created. Each group was awarded a grade. The higher the fitness function values in a group, the higher the grade, with the highest grade awarded being 10. The group that contained the lowest values of fitness function was awarded grade 1.

New aerofoils were created using the genes of the analysed ones, and all of the aerofoils in a generation had at least one chance of being used as providers of genes for the next generation of aerofoils. The likelihood of each aerofoil to be used as a gene provider or parent was established based on its grade. A function to represent this probability was developed and is presented below:

$$P_S = 11 - x;\ x \in \mathbb{Z},\ P_S \in \mathbb{N} \quad \ldots(4)$$

$$x = \begin{cases} y, y \geq 1 \\ 1, \text{y} \leq 1 \end{cases};\ x, y \in \mathbb{Z} \quad \ldots(5)$$

$$y = \begin{cases} z^{A_f}, z^{A_f} \leq 10 \\ 10,\ \text{z}^{A_f} \geq 10 \end{cases};\ y, z \in \mathbb{Z} \quad \ldots(6)$$

$$z = \begin{cases} \underline{\lambda}, \lambda \geq 0 \\ \\ \overline{\lambda}, \lambda \leq 0 \end{cases};\ \lambda \in \mathbb{R};\ z \in \mathbb{Z}$$

$$\lambda = \delta \cdot 10^{\frac{1}{A_f}};\ \text{random}\ \delta \in [0, 1]; \quad \ldots(7)$$

where P_S is the probability of selection and A_f represents the attraction factor given by the user, which is set at 2, for the present case. The attraction factor shows with how much an individual with a high grade is more attractive to become a parent. The P_S function returned values between 1 and 10, corresponding to the grades associated to the aerofoils. The value of P_S was compared to the grades allocated to each aerofoil based on the fitness function. All aerofoils whose grades were equal to the P_S value were grouped and one of them was selected at random to play the role of parent. The process was repeated until all the required parents were chosen. In order to solve the problem of aerofoil shape modification, two parents were considered sufficient for each new individual aerofoil.

The new set of aerofoils was created using *cross-over* and *mutation* functions applied to the randomly chosen parents. Two *cross-over* functions were used, depending on the number of aerofoil generations deemed necessary to achieve the optimum in drag reduction. It was observed that, for this algorithm, the optimum region was reached after the analysis of ten generations of aerofoils using a simple *cross-over* function, which mixed equal shares of the genes. To avoid finding a local optimum instead of a global one, another *cross-over*

https://doi.org/10.1017/aer.2016.30 Published online by Cambridge University Press

function was added and it affects the generations beyond the tenth. This function was based on the simulated binary *cross-solver* technique[25] and used a random number in the following manner:

$$\text{child} = \begin{cases} \text{child}_{\text{equalshare}}, \text{generation} \leq 10 \\ \text{child}_{\neq\text{equalshare}}, \text{generation} > 10 \end{cases} \quad \ldots(8)$$

$$\text{child}_{\text{equalshare}}(\text{gene}_i) = \text{gene}_{i\_\text{parent}_j}; \quad i \in [1, \text{number\_of\_genes}],\ j \in [2, \text{number\_of\_parents}] \quad \ldots(9)$$

$$\text{child}_{\neq\text{equalshare}} = \begin{cases} \frac{1}{2} \cdot (1+\delta) \cdot \text{gene}_{i\_\text{parent}_j}, \delta \geq 0.5 \\ \frac{1}{2} \cdot (1+\delta) \cdot \text{gene}_{i\_\text{parent}_{j+1}}, \delta < 0.5 \end{cases}; \quad \text{random}\ \ \delta \in [0, 1];\ i \in [1, \text{number\_of\_genes}],\ j \in [2, \text{number\_of\_parents}] \quad \ldots(10)$$

The *mutation* affected a percentage of the aerofoils resulted from the *cross-over* function(s), and changed the values of the genes with a percentage of *mutation*. Two variables were used to achieve *mutation*. One variable gave the 'chance of mutation', which gave a percentage of the number of aerofoils in a generation that would be affected by the mutation process and was always a very small value (in percentage) that did not lead to a degeneration of the optimisation. For our problem, the chance of mutation was set at 0.01% of the number of aerofoils in a set. The second variable was the 'percentages of mutation' that gives the amount of genes, which were to be modified. This variable must always be sufficiently small, so that the modified value of the gene does not surpass the upper or lower limits, if there are any imposed. In our case, the percentage of mutation was set at a maximum of 2% of the value of the genes it affected.

A final step in the genetic algorithm that ensures a rapid convergence towards the optimum was the *tournament*. The *tournament* is a process in which some of the worst members of the current generation of airfoils are replaced with some of the best members from the previous aerofoil generation. This process gives more chances to those aerofoils that are close to the optimum to contribute with their genes to the next set of aerofoils. For our problem, the maximum number of aerofoils and generations used was 40 aerofoils per generation for a total of 20 generations. The maximum number of generations was imposed after convergence tests have shown that, for more than 20 generations and 40 aerofoils, no extraordinary modifications in the shape of the optimal aerofoils occur.

Figure 2 presents the 'step by step' process of optimisation from input, which contains the original aerofoil coordinates, the flight and optimisation conditions, to the result, which contains the optimised aerofoil coordinates and its pressure and aerodynamic characteristics.

2.4 XFoil code description

The code used for the calculation of the two-dimensional aerodynamic characteristics of the wing's control sections is XFoil, version 6.96, developed by Drela and Youngren[26]. The XFoil code was chosen because it has proven its precision and effectiveness over time, and because its rapid convergence. In XFoil, inviscid calculations were performed using a *linear vorticity stream function panel method,* to which a Karman-Tsien compressibility correction[27] was added, allowing for the obtaining of good predictions of subsonic flow. For the viscous flow calculations, XFoil uses a two-equation lagged dissipation integral boundary layer formulation[28] and incorporates the e^n transition criterion[29]. The flow in the boundary layer and in the wake interacts with the inviscid potential flow by using the *surface transpiration model*.

https://doi.org/10.1017/aer.2016.30 Published online by Cambridge University Press

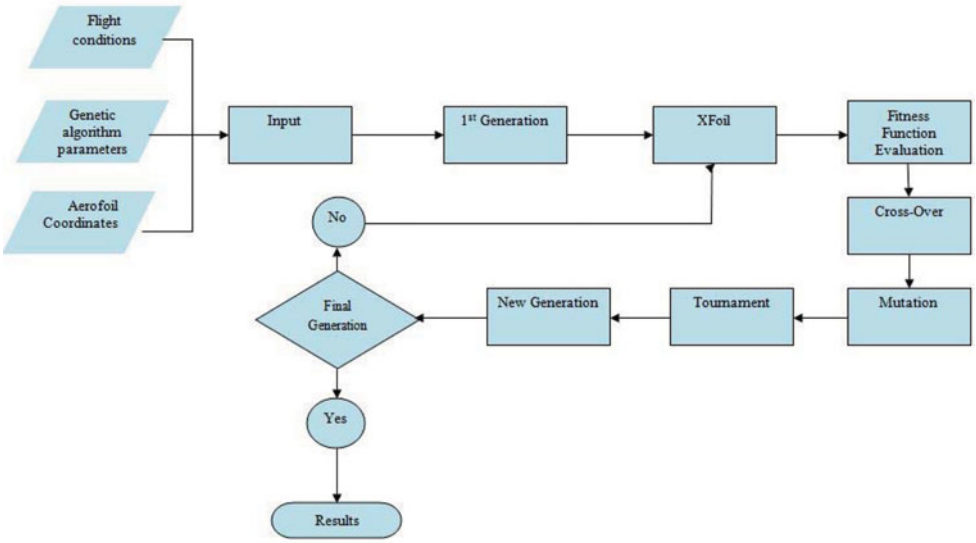

Figure 2. (Colour online) Schematic of the genetic algorithm/XFoil coupled software.

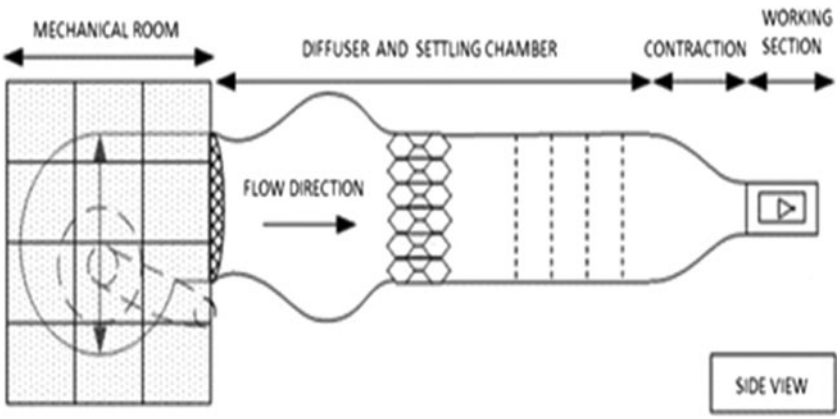

Figure 3. Components of the Price-Païdoussis wind tunnel (reproduced from Ref. 30).

3.0 PRICE-PAÏDOUSSIS SUBSONIC WIND TUNNEL

Before the presentation of the wing model design and manufacturing in the following section, a short presentation of the Price-Païdoussis wind tunnel is given, as the dimensions of the test chamber and some of the characteristics of the wind tunnel have an impact on both models' dimensions.

The Price-Païdoussis wind tunnel is an experimental facility at the École de Téchnologie Supérieure under the supervision of Professor Ruxandra M. Botez, head of the LARCASE laboratory (Aeronautical Research Laboratory in Active Control, Avionics and Aeroservoelasticity) and the Canada Research Chair for Aircraft Modeling and Simulation Technologies. The Price-Païdoussis facility is a 12 m blow-down subsonic wind tunnel. The main components of the wind tunnel are represented in Fig. 3 and its dimensions in Fig. 4.

https://doi.org/10.1017/aer.2016.30 Published online by Cambridge University Press

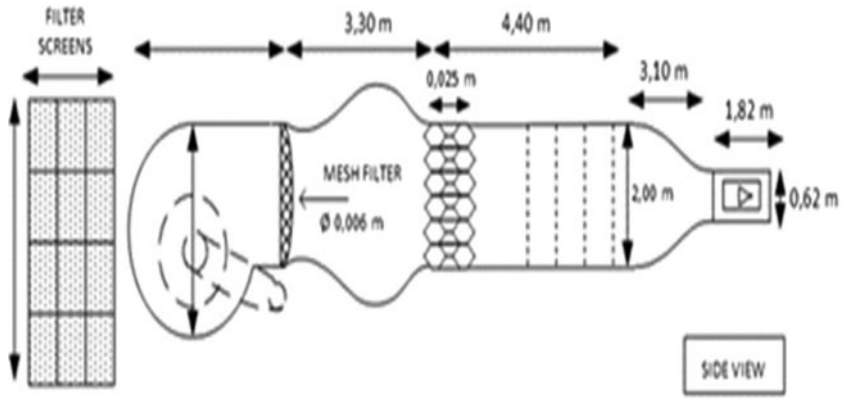

Figure 4. Dimensions of the Price-Païdoussis wind tunnel (reproduced from Ref. 30).

Figure 4a. (Colour online) Wing model installed in the wind-tunnel chamber.

The wind tunnel is powered by a 40 HP, 67 Amps electrical engine, from North Western Electric Co and is fitted with a double impeller centrifugal fan. The maximum speed it can reach is approximately 61 m/s or 0.18 Mach in the smaller of the two test chambers that complete the wind tunnel. The chambers are made of wood, with Plexiglas removable doors on each side, for greater accessibility to the models installed inside. The main test chamber has dimensions of $0.62 \times 0.91 \times 1.83$ m (H × W × L) and the speeds that can be sustained in it are around 40 m/s, equivalent to 0.12 Mach, with a maximum Reynolds number of 2.4 m.

https://doi.org/10.1017/aer.2016.30 Published online by Cambridge University Press

The smaller of the two chambers is 0.31 × 0.61 × 1.22 m (H × W × L) and can sustain the maximum speed of the wind tunnel and a Reynolds number of 3.5 m. Reynolds numbers were calculated using a chord of 0.8 m, which is the maximum chord that a model can have, in order to be tested in either of the test chambers.

The wind tunnel's turbulence level is approximately 0.3, corresponding to a critical amplification factor of 5.5 for the XFoil analysis. The correspondence between the flow turbulence level (T) and the critical amplification factor (N), used in the 'e^n' transition estimation method, was given by Mack's formula[30]:

$$N = -8.43 - 2.4\ln(T) \quad \ldots(11)$$

A. Ben Mosbah et al[31] presented a detailed description of the wind-tunnel components and flow measurements, for ISO certification.

In order to decide which one of the test chambers should be used, it was necessary to determine the dimensions of the models. The requirements for the models dimensions were determined by the requirements for a bi-dimensional wing model, as recommended by J. Borlow, W. Rae and A. Pope[32]. In addition, the models' dimensions were determined by the requirements of the active morphing wing model developed in the second phase of the project. The active morphing model included a morphing mechanism and pressure sensor cables installed inside the model, which indicates the need for a model large enough to house them.

Based on these considerations, the larger testing chamber was chosen. The final dimensions of the models were calculated using the testing chamber length and width, the thickness of the aerofoil and the formulas indicated in Ref. 32. Thus, the wing models have a span of 0.6 m and a chord of 0.244 m, and their thickness is 35 mm. This thickness was considered more than enough to house the pressure taps used for pressure measurement on the rigid wing models in the first phase of the project, presented in this paper, and sufficiently large to house most of the morphing mechanism of the active morphing wing developed in the second phase of the project.

4.0 MANUFACTURING OF THE RIGID WING MODELS

As mentioned in the first section, the wings were manufactured from fibreglass-epoxy resin composite material, which was selected because it meets several of the requirements for the morphing area material. The proposed materials were aluminium, carbon-Kevlar and unidirectional TG-18_U glass fibre combined with epoxy resin (fibreglass). The criteria, on which the material was chosen, were based on mechanical properties as well as on the financial and technological availabilities. The Carbon-Kevlar material was successfully used during the CRIAQ 7.1 project and it was considered as a possible candidate, but it was not chosen because it was not easily available and reproducible and also because it was considered more beneficial to explore other materials and optimisation techniques. The aluminiums' intrinsic mechanical properties makes it an unlikely choice for a flexible skin that needs to change shape while minimising the forces needed for the actuation system, therefore it is difficult to optimise aluminium and the amount of time needed for such a process was considered too high. The final weight of the model was also one of the parameters considered in the choice of materials.

The final decision was to create an optimised uni-directional TG-18_U fibre-epoxy resin composite best-suited to the project's needs. The fibers used were J.B. Martin's UD TG-9U fibres infused with epoxy at a fibre volume fraction of 50%. The optimisation, of the number of

https://doi.org/10.1017/aer.2016.30 Published online by Cambridge University Press

Table 1
Properties of the composite components[33]

Property	Unit (SI)	Epoxy/Glass UD	Bonding Paste
E1	GPa	48	4
E2	GPa	13	-
G12	GPa	4.75	1.2
S1T	MPa	848	62
S2T	MPa	62	-
S1C	MPa	579	100
S2C	MPa	239	-
S12	MPa	76	13.35
ν12	-	0.26	0.31

plies along the span and chord of the wing and the direction of the glass fibres, was carried out using the Hyperworks software. The optimisation process and the evaluations of the resulted composite are presented by F. Michaud et al[33].

Table 1 presents several characteristics of the composite material that was used for the manufacturing of the wing models.

The composite optimisation process took into account the deformations obtained with the aerodynamic optimisation software in a multidisciplinary loop between the aerodynamic and structural parts of the project.

The goal of the material optimisation process was to match the structural shape to the theoretical shape provided by the aerodynamic optimisation.

The composite material for the rigid models was found to have a constant thickness of 0.25 mm per ply, four plies in both the span and the chord lengths, while the glass fibres were oriented at 0° and 90° to insure sufficient rigidity in both directions of the chord and span. The composite material was stiffened with an epoxy-based bonding paste.

Initially, it was planned to use the composite material only for the region between 10%c and 70%c on the upper-surface (where c represents the chord of the wing), but, due to the complications in manufacturing a small model from two different materials and in the interest of observing the behaviour of the composite material, it was decided to use it for the full surface of the wing models.

Several materials (metal, wood, composite, etc.) were proposed for the manufacturing of the wing models moulds. Since the models were made one after another and the moulds were to be used for the manufacturing of the morphing wing in the second phase of the project, the material from which the moulds were made must provide precision and reliability for the manufacturing process without deteriorating. Thus, the moulds were machined from aluminium blocks and the base of the wing models was made from solid steel that was cut to shape with laser tools.

Two moulds were created for each wing model – one for the upper surface part and one for the lower surface part of the wing – and after the installation of the pressure tap's cables, the two parts were assembled together using EPIKOTE Resin MGS BPR 135G.

The manufacturing process, the assembly and the finishing of the models was done at ETS in our LARCASE laboratory.

The wings were placed in the wind-tunnel testing chamber with tufts (small wool fibres) placed on the upper surface and were tested to verify that the effects of the wing model edges

https://doi.org/10.1017/aer.2016.30 Published online by Cambridge University Press

were attenuated and disappeared at the centre of the wing. This meant that the flow around the wing had bi-dimensional characteristics in the region where the pressure sensors were installed.

A detailed description of the realisation of the rigid wing models for the Price-Païdoussis wind tunnel was given in R. Caléstreme's Master's thesis[34].

The testing of the wing models in the Price-Païdoussis wind tunnel confirms that the simple optimisation of the composite was sufficient for this phase of the project. The material has resisted to the aerodynamic forces developed by the wind tunnel at the highest speed and angle-of-attack without any visible deterioration.

5.0 PRESSURE MEASUREMENT SYSTEM

As mentioned earlier, the pressure in the wind tunnel was measured using pressure taps connected to an AeroLab PTA (pressure transducer array) measurement system. These pressure taps were chosen because they are used in experimental set-ups and represent an economical solution[35,36].

The AeroLab PTA system was chosen to record the data without the inaccuracies of interpretation inherent to traditional fluid-filled multi-tube manometers, which need manual recording. The PTA is an adaptable and configurable system that comes completely fitted with pressure sensors that allows the measurement of the absolute atmospheric pressure between 800 and 1200 mbar and absolute pressure between 0 and 10 bar with an accuracy of $\pm 0.05\%$ of the basic range and a resolution of 0.002% of the basic range. The connecting vinyl tubes, from the taps on the upper and lower surfaces of the wing, needed to be connected to the 24 pressure fittings installed on the PTA system box, which was equipped with its own, easy to use, executable program, LabView. More details on this PTA system can be found on the AeroLab site[37].

The most convenient method of installing the pressure sensors was to integrate them, using flexible connecting vinyl tubes connected to a cavity on the model surface at one end and the pressure measurement system at the other end. This method was chosen because it eliminated the need to disassemble the models after manufacturing, and to assemble them again in order to change a pressure sensor without damaging other sensors in the process.

The holes in the upper and lower model skins had to respect a number of constraints. The literature in this domain[38-40] states that the dimensions of the holes should be between 0.5 and 3 mm in diameter, the ratio between their lengths and diameters must be between 5 and 15, and the cavity for the connecting vinyl tubes should have a greater diameter than the hole. The last condition, when respected, will minimise the length of the hole's channel. These three conditions were necessary to obtain good precision in measurements and to avoid parasitic effects, for example, turbulence in the cavity, which would change the measured values. In our case, the holes had a diameter smaller than 1 mm; thus, it was not necessary to respect all of the above conditions, because for a hole with a very small diameter the geometry and inclination of the hole's channel would have no effect on the measurements, thereby facilitating the process of puncturing the holes during the skin manufacturing process.

Twenty pressure taps were installed on the upper and lower surfaces of the original wing model. Eighteen were installed on the upper and lower surfaces of the optimised wing model. The wing reproducing the original shape of the ATR 42 aerofoil has 14 taps on the upper surface and six taps on the lower surface, while the model reproducing the optimised shape

https://doi.org/10.1017/aer.2016.30 Published online by Cambridge University Press

Table 2
Pressure taps positions on the upper and lower surface of the rigid original model

Original Rigid Wing model upper-surface														
Chord position (%)	5	10	15	20	25	30	32.5	35	37.5	40	45	50	60	70
Chord position (mm)	12.2	24.4	36.6	48.8	61	73.2	79.3	85.4	91.5	97.6	109.8	122	146.4	183
Original Rigid Wing model lower-surface														
Chord position (%)	2.77	10	20	40	60	80								
Chord position (mm)	6.8	24.4	48.8	97.6	146.4	195.2								

Table 3
Pressure taps positions on the upper and lower surface of the rigid optimised model

Optimised Rigid Wing model upper-surface														
Chord position (%)	5	10	15	20	25	30	35	40	45	50	55	60	65	70
Chord position (mm)	12.2	24.4	36.6	48.8	61	73.2	85.4	97.6	109.8	122	134.2	146.4	158.6	170.8
Optimised Rigid Wing model lower-surface														
Chord position (%)	3.1	10	20	30										
Chord position (mm)	7.6	24.4	48.8	73.2										

has 16 taps on the upper surface and only four on the lower. Fewer pressure taps were used for the lower surface because the upper surface was considered of more importance because of the morphed region. Tables 2 and 3 present the distribution of the pressure taps on both wings. In Table 2, it can be observed that the distribution of the pressure taps on the upper surface of the rigid wing model has a variable step in the chord direction. The variable step was chosen after analysing the numerically calculated transition point positions. On the optimised model (Table 3), the step between pressure taps is maintained constant in order to observe how much the position of the pressure taps, determined in function of the numerical transition, influences the accuracy of determining the experimental transition.

Figures 5(a) and 5(b) present the wind-tunnel set-up for the wing models.

Before the installation of both models in the wind tunnel, the positions of the pressure taps and the dimensions of the holes were measured and compared with the theoretical values from the CAD files. The measurements were done using a ‘contour gauge’ with a precision of 0.1 mm and an ‘electronic caliper’, and the results show small, negligible differences between the theoretical and the actual values.

https://doi.org/10.1017/aer.2016.30 Published online by Cambridge University Press

Figure 5(a). (Colour online) Optimised wing model installed inside the test chamber ready for testing.

Figure 5(b). (Colour online) Original rigid wind model installed in the wind-tunnel test chamber and connected to the AEROLAB measurement system.

https://doi.org/10.1017/aer.2016.30 Published online by Cambridge University Press

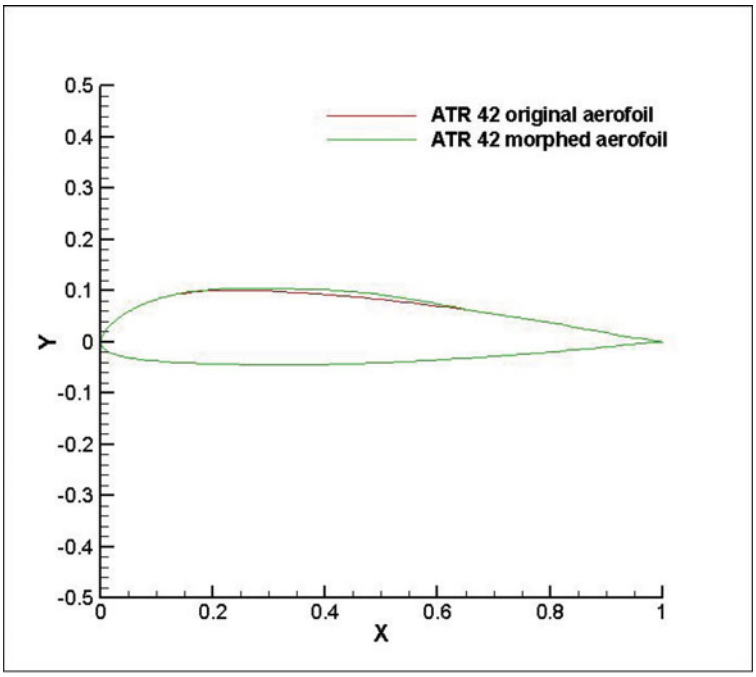

Figure 6. (Colour online) Optimised ATR 42 aerofoil shape vs. Original ATR 42 aerofoil shape.

6.0 RESULTS

The numerical analysis results were compared with the experimental data, for the two rigid models discussed above, for the pressure distributions along the chord and for the second derivative of the pressure coefficient. One of the objective of the first phase of the project, presented in this paper, was to ascertain whether wind-tunnel correction were needed. From the analysis of the experimental data and comparison with the numerical results no wind-tunnel corrections (wall effects) were needed for the pressures or the angles of attack used for the experiment; as the validation of numerical versus experimental data gave very good results for the subsonic Price-Païdoussis wind tunnel.

6.1 Wind-tunnel test cases

As mentioned in the previous sections, there were two rigid wing models. The first model was a representation of the original aerofoil, while the second was the reproduction of an optimised version of the original aerofoil. The aerofoil was optimised for Mach number of 0.1 and angle-of-attack of 0° using two control points situated at 30% and 50% of the chord. Figure 6 shows the shapes of the two aerofoils used for the development of the wing models.

The optimisation function used was described in section 2.3 on optimisation (eq. 1.2). Forty randomly modified aerofoils based on the original ATR 42 aerofoil and 20 generations were needed to obtain the final aerofoil shape that was used for manufacturing.

The numerical and experimental tests were done to validate the aerodynamic and composite material optimisation procedures and to prove that the modification of the upper

https://doi.org/10.1017/aer.2016.30 Published online by Cambridge University Press

Table 4
Numerical and experimental test cases for both rigid models

Case	Speed(m/s)	Mach	Angle-of-attack(°)	Reynolds No.
1	27.2	0.08	−2	4.30E+05
2			−1	
3			0	
4			1	
5			2	
6	30.6	0.09	−2	4.85E+05
7			−1	
8			0	
9			1	
10			2	
11	34	0.1	−2	5.40E+05
12			−1	
13			0	
14			1	
15			2	

surface of the ATR-42 aerofoil (one aerofoil shape presented as optimised wing model) produces improvements in the transition location, and implicitly in the value of the drag coefficient.

Table 4 presents a complete list of the tests performed for both the experimental setup in the Price-Païdoussis wind tunnel and the numerical analysis with XFoil.

In this section, only the results obtained for three test cases, 2, 8, and 15 (Table 4), are presented and discussed, for different speeds and angles of attack, because of the similarity of the results obtained for the group of cases. In the final part of the results section, the numerical results for all test cases are given in Tables 7(a)-7(d).

Figures 7-9 show a comparison between the pressure distribution calculated with XFoil and the pressure distribution determined from wind-tunnel experimental data for each of the rigid models. For each set of figures, (a) represents the comparison between the experimental and numerical data for the original model, (b) represents the comparison between the experimental and numerical data for the optimised model, and (c) represents the comparison between the experimental data for both models.

6.2 Analysis of the pressure distributions

Case 2 – Analysis and testing for Mach number of 0.08 and angle-of-attack of −1°
Case 8 – Analysis and testing for Mach number of 0.09 and angle-of-attack of 0°
Case 15 – Analysis and testing for Mach number 0.1 and angle-of-attack of 2°

From the results presented in Figures 7-9(a and b) it was observed that the experimental data agrees with the XFoil predictions without applying any wind-tunnel corrections, which confirms that at very small speeds and angles of attack, 2D wind-tunnel corrections are not necessary. On the upper surface, the good agreement between the experiment and the numerical prediction was due to the sufficiently high number of pressure taps installed, and it was observed that the pressure taps' readings closely follows the XFoil predicted curve. On

https://doi.org/10.1017/aer.2016.30 Published online by Cambridge University Press

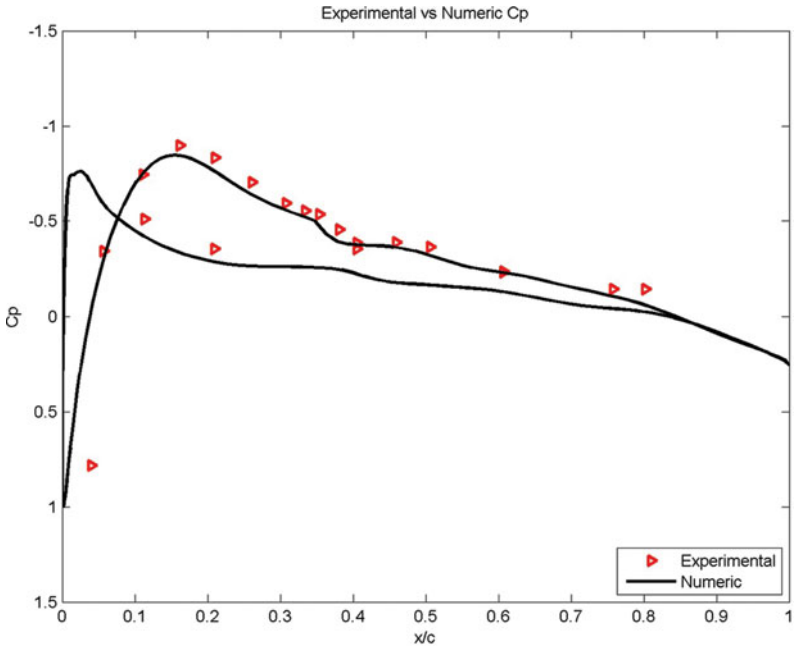

Figure 7(a). (Colour online) Comparison, for the original model, of the pressure distribution calculated with XFoil vs. experimental pressure distribution.

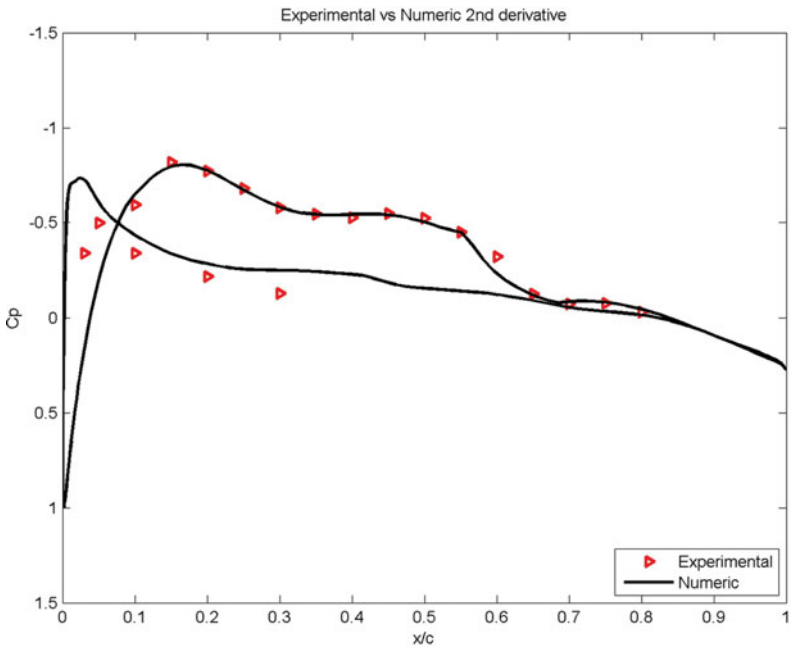

Figure 7(b). (Colour online) Comparison, for the optimised model, of the pressure distribution calculated with XFoil vs. experimental pressure distribution.

https://doi.org/10.1017/aer.2016.30 Published online by Cambridge University Press

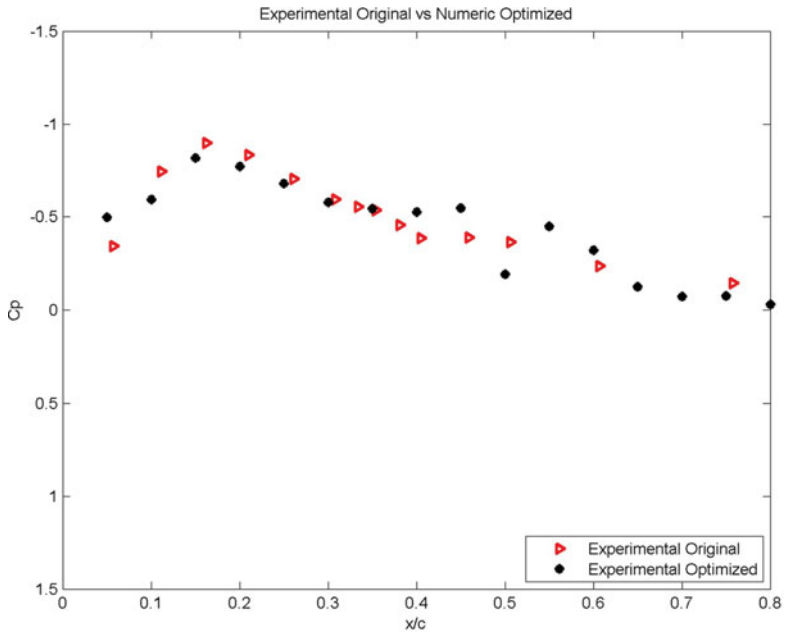

Figure 7(c). (Colour online) Comparison of the experimental pressure distribution for the optimised model vs. experimental pressure distribution for the original model.

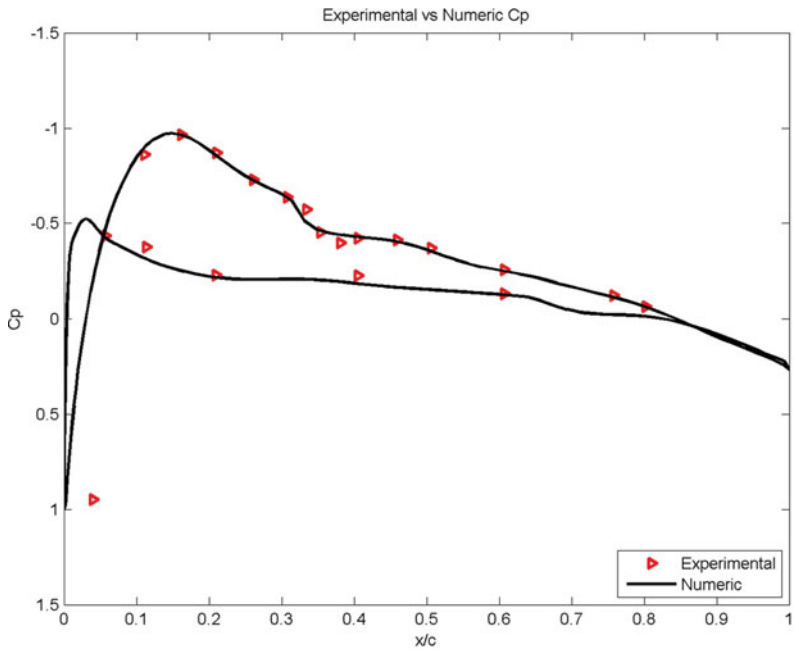

Figure 8(a). (Colour online) Comparison, for the original model, of the pressure distribution calculated with XFoil vs. experimental pressure distribution.

https://doi.org/10.1017/aer.2016.30 Published online by Cambridge University Press

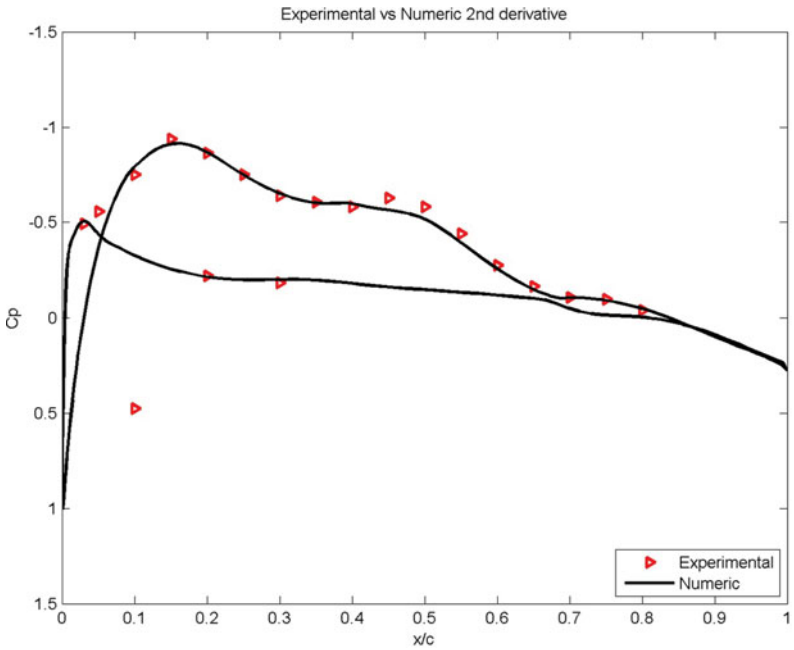

Figure 8(b). (Colour online) Comparison, for the optimised model, of the pressure distribution calculated with XFoil vs. experimental pressure distribution.

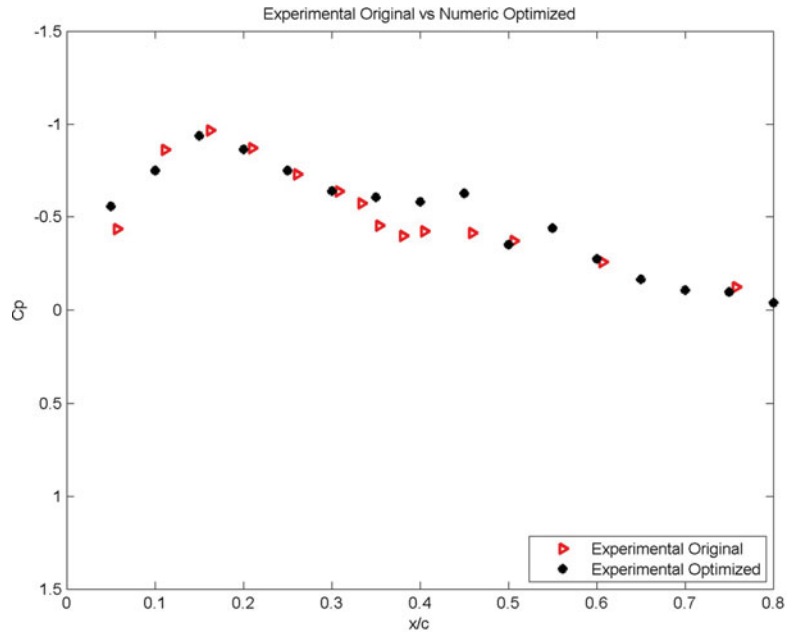

Figure 8(c). (Colour online) Comparison of the experimental pressure measurements for the optimised model vs. the experimental pressure measurements for the original model.

https://doi.org/10.1017/aer.2016.30 Published online by Cambridge University Press

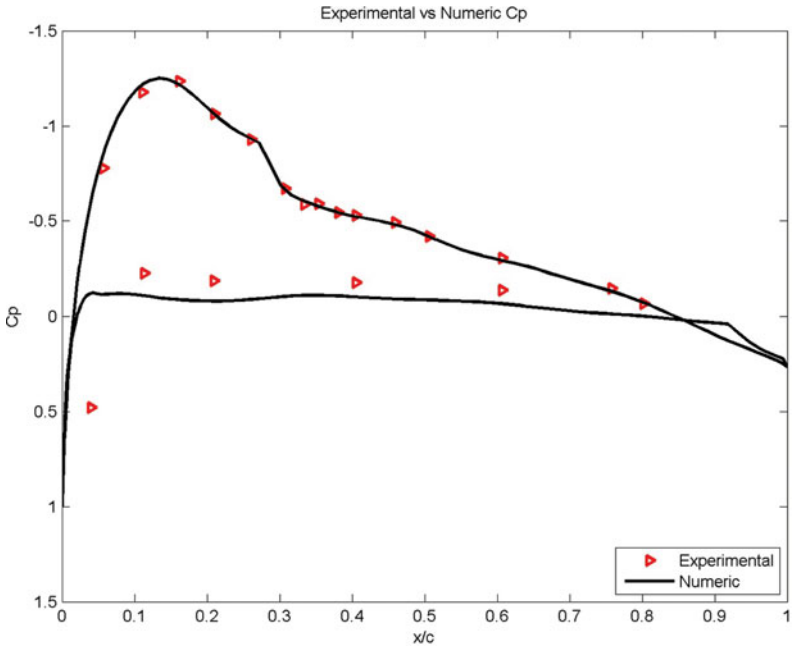

Figure 9(a). (Colour online) Comparison, for the original model, of the pressure distribution calculated with XFoil code vs. experimental pressure distribution.

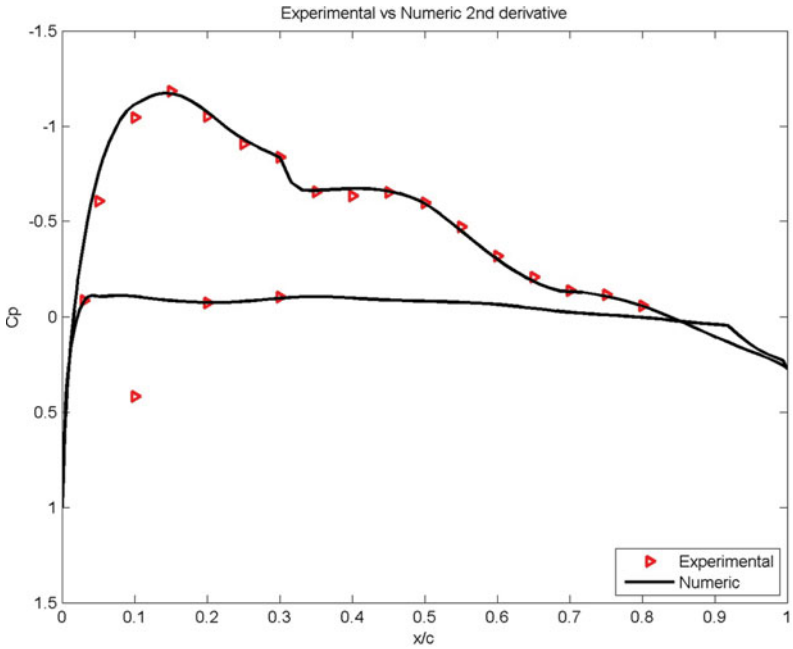

Figure 9(b). (Colour online) Comparison, for the optimised model, of the pressure distribution calculated with XFoil code versus experimental pressure distribution.

https://doi.org/10.1017/aer.2016.30 Published online by Cambridge University Press

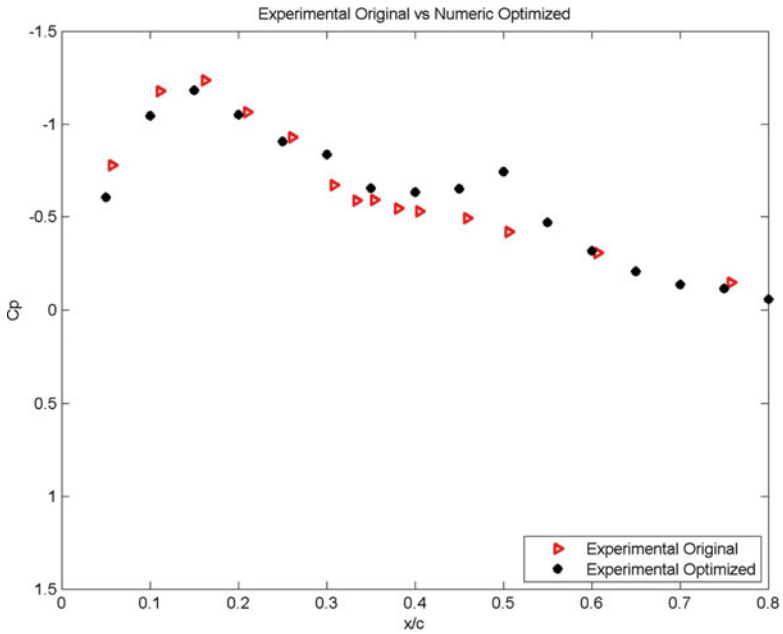

Figure 9(c) (Colour online) Comparison of the experimental pressure measurements for the optimised model vs. the experimental pressure measurements for the original model.

the lower surface, the pressure taps' readings do not follow the shape of the numerical curve as closely. This was due to the small number of sensors installed, to a blocking of the second pressure sensor on the lower surface, but, since the most accurate readings were needed on the upper surface, where the optimisation took place, the experimental data obtained for the lower surface was considered sufficient.

Figures 7-9(c) show the comparison between the experimental results of the original shape model and the optimised shape model for each of the cases. It can be seen that even a small difference in shape induced a visible change in the pressure distributions. Numerical percentages of the improvements of the transition position for each of the cases are presented in Tables 7(a)-7(d).

6.3 Second derivative analysis of the pressure data for transition estimation

Figures 10-12 present the analysis of the second derivative of the pressure coefficient measurements, which allowed us to predict the transition position from the experimental data without requiring expensive or complicated equipment.

The transition of the boundary layer from laminar to turbulent has been an important topic in aerodynamics since Osborne Reynolds[41] 1883 publication on this subject. Today there is still no complete transition theory; instead, empirical or semi-empirical correlations and expensive wind-tunnel measurements are used to determine transition.

The classical approach for determining transition in numerical aerodynamic calculations is based on iterative methodology, by combining a panel code with a boundary layer code. To be able to simulate the transition region, the boundary layer code needs to be coupled with a

https://doi.org/10.1017/aer.2016.30 Published online by Cambridge University Press

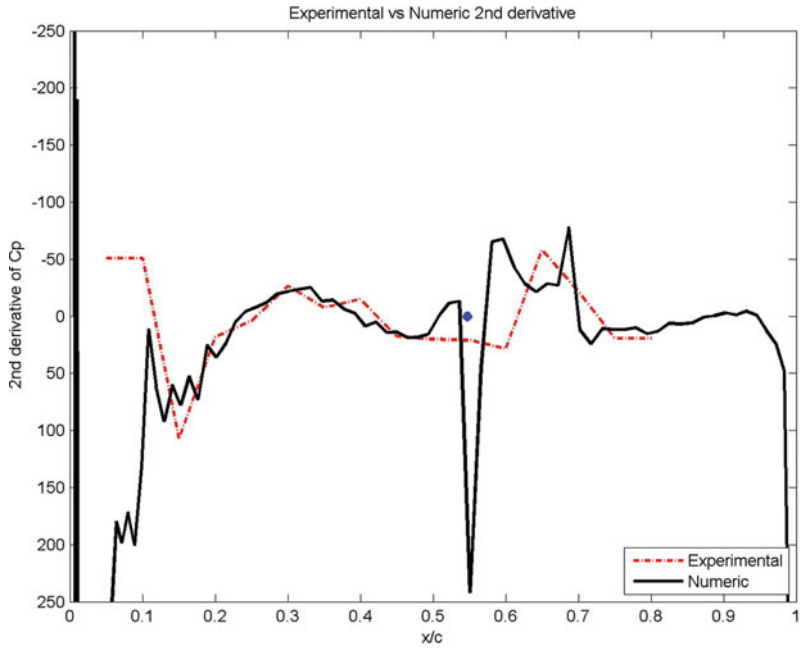

Figure 10(a). (Colour online) Variation of the second pressure derivative using XFoil pressure distribution, experimental pressure distribution and the XFoil predicted transition point, for the optimised model.

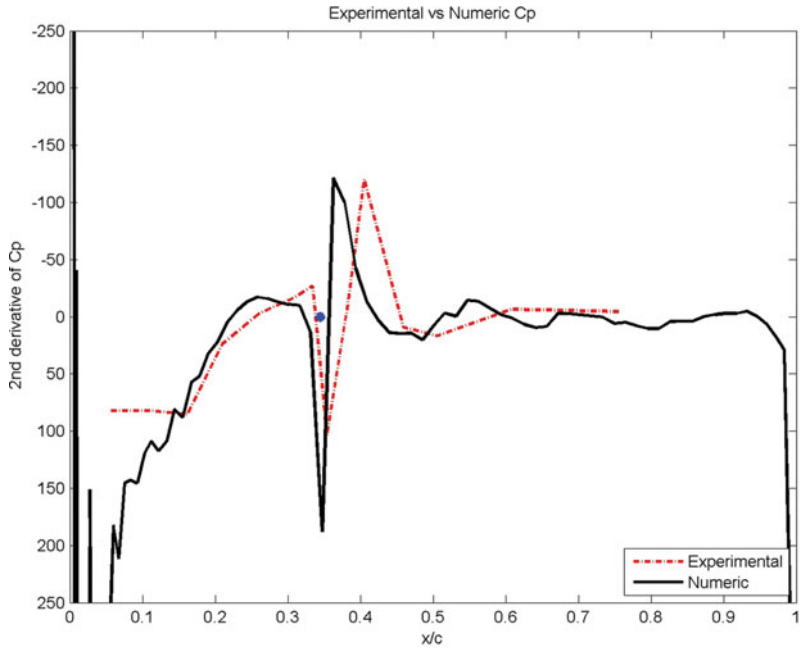

Figure 10(b). (Colour online) Variation of the second pressure derivative using XFoil pressure distribution, experimental pressure distribution and the XFoil predicted transition point for the original model.

https://doi.org/10.1017/aer.2016.30 Published online by Cambridge University Press

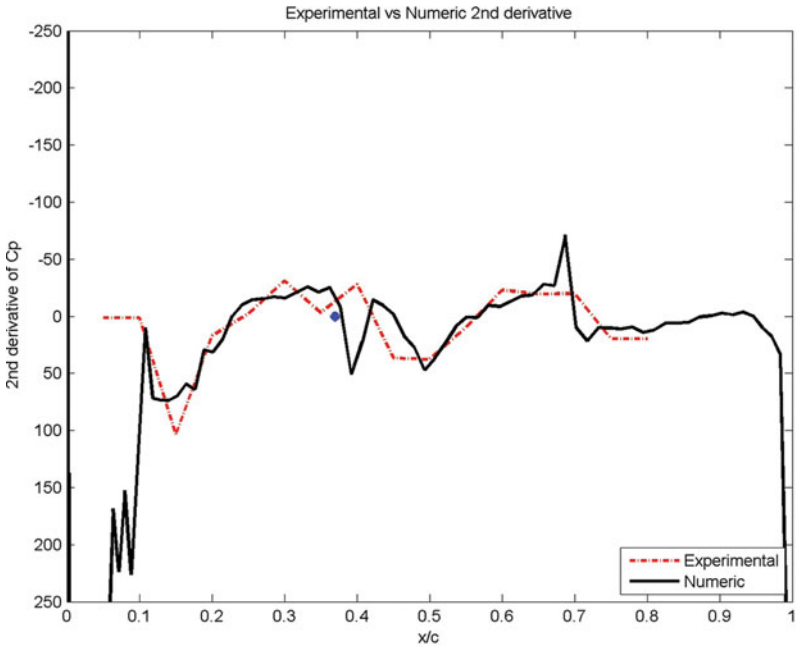

Figure 11(a). (Colour online) Variation of the second pressure derivative using XFoil pressure distribution, experimental pressure distribution and the XFoil predicted transition point for the optimised model.

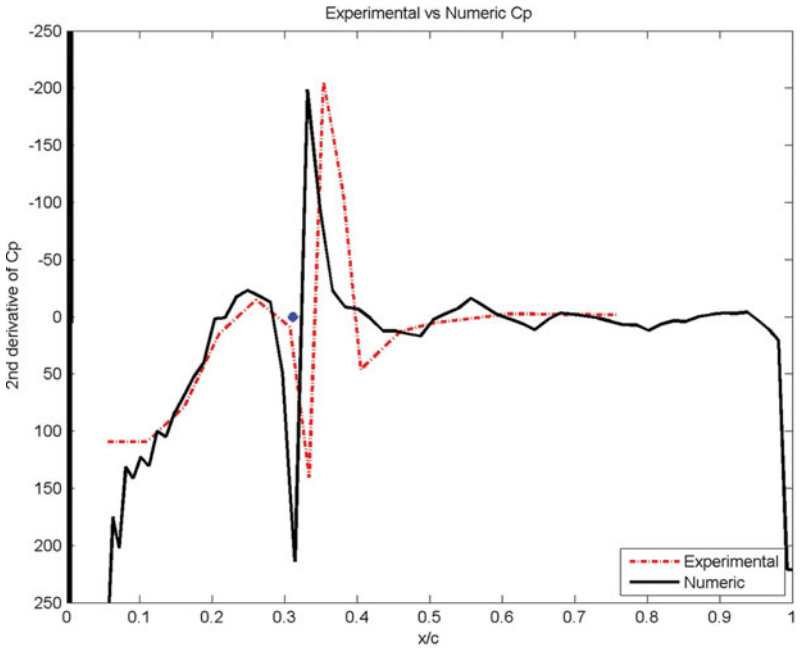

Figure 11(b). (Colour online) Variation of the second pressure derivative using XFoil pressure distribution, experimental pressure distribution and the XFoil predicted transition point for the original model.

https://doi.org/10.1017/aer.2016.30 Published online by Cambridge University Press

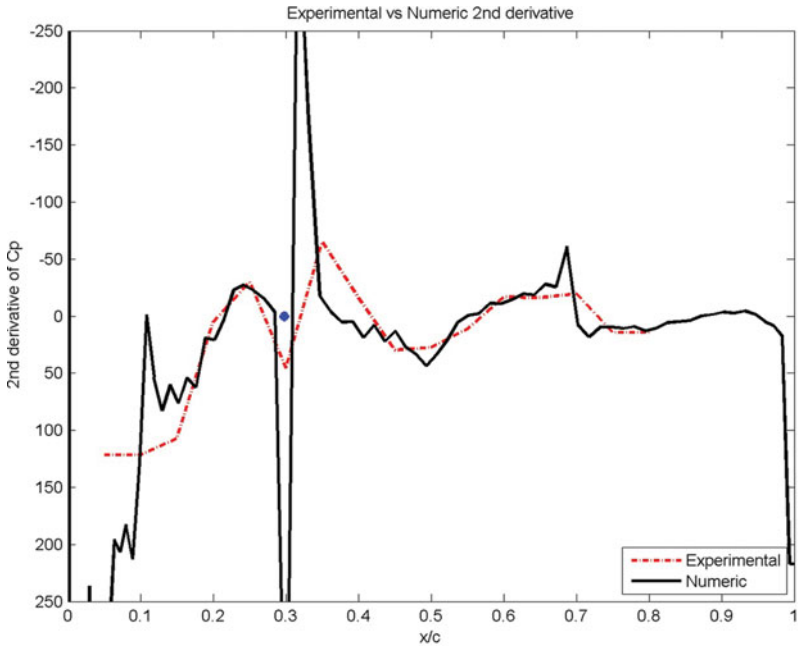

Figure 12(a). (Colour online) Variation of the second pressure derivative using XFoil pressure distribution, experimental pressure distribution and the XFoil predicted transition point for the optimised model.

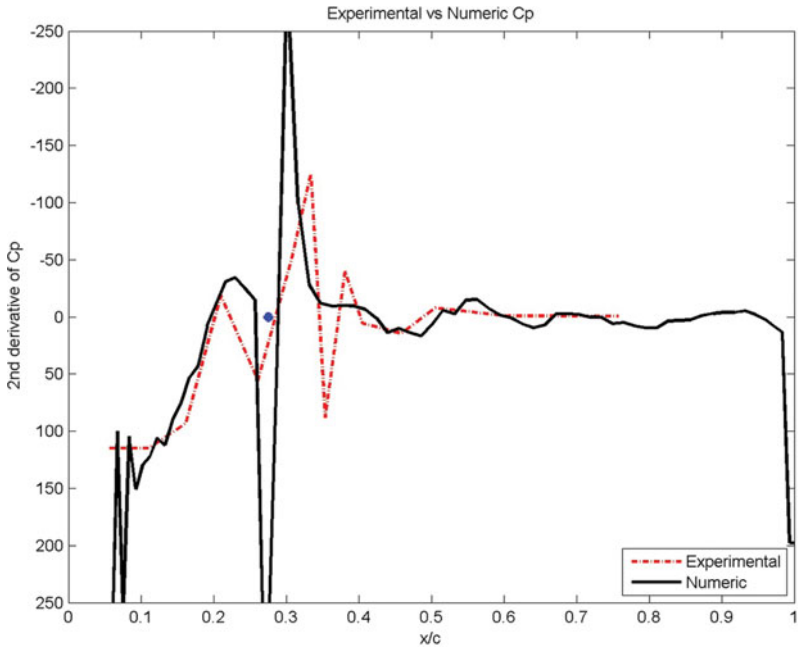

Figure 12(b). (Colour online) Variation of the second pressure derivative using XFoil pressure distribution, experimental pressure distribution and the XFoil predicted transition point for the original model.

https://doi.org/10.1017/aer.2016.30 Published online by Cambridge University Press

stability code based either on linear stability theory or on wind-tunnel-derived correlations. However, this approach only works for cases where classical boundary layer theory[42] holds true, which restricts it to cases with attached flow. More recently, codes such as ANSYS Fluent[43] have introduced transition calculation in conjunction with modern aerodynamic methods, but, even here, the methods used to determine transition are actually empirical correlations. A different way of determining transition was proposed by Silisteanu and Botez[44]. They use the refining of the grid as the starting point to obtain accurate information on the boundary layer.

The most commonly known empirical correlations are the 'Granville' method[45], the 'one-step' method of Michel[46], the Wazzan method[47], and the e^n method implemented in XFoil solver that was used for our numerical calculations.

Practically, even if no general transition theory exists, as of yet, there are a number of methods that can be used to numerically determine the transition position with very good accuracy[48-51].

From an experimental point of view, the detection of the transition region on a wing in a wind tunnel needs expensive equipment during the tests, e.g. an infrared scanner, highly sensitive optical sensors, Kulite pressure sensors, etc., as well as post-processing equipment for the resulted experimental data. In an experimental set-up, such as the one presented in this paper, in which a reduced scale wing model was fitted with pressure taps, it was not possible to have all that equipment, but the estimation the transition position on the upper surface with a reasonable degree of accuracy was necessary and it was done. Thus, pressure data was collected during our experiment, and this data was used to determine, with a certain degree of accuracy, the region on the upper surface where transition occurs.

The flow transition can be detected on an XFoil pressure distribution plot by a point with a high gradient in the local pressure. This detection is shown analytically in the equation of motion (12) of the boundary layer to which wall conditions are applied.

$$\rho\left(\frac{\partial u}{\partial t}+\frac{u\partial u}{\partial x}+\frac{v\partial u}{\partial y}\right)=\frac{-\partial p}{\partial x}+\frac{\partial}{\partial y}\left(\mu\frac{\partial u}{\partial y}\right)$$

wall conditions

$$u=v=0 \text{ at } y=0 \qquad \ldots(12)$$

The results are given in Equation (13).

$$\frac{\partial p}{\partial x}=\mu\frac{\partial^2 u}{\partial y^2}\bigg|_{y=0} \qquad \ldots(13)$$

When the pressure gradient is positive, a deceleration of the flow occurs until it becomes reversed.

The transition onset is associated with the maximum of the velocity streamline curvature and the maximum curvature in the pressure plot. To determine the maximum velocity streamline curvature, it is sufficient to derive Equation (13) one time with respect to x.

$$\frac{\partial}{\partial x}\left(\frac{\partial p}{\partial x}\right)=\frac{\partial}{\partial x}\left(\mu\frac{\partial^2 u}{\partial y^2}\bigg|_{y=0}\right) \qquad \ldots(14)$$

https://doi.org/10.1017/aer.2016.30 Published online by Cambridge University Press

It was observed that the result corresponds to the second derivative of the pressure, which, in turn, corresponds to the 'maximum of the pressure curvature'.

The laminar separation point was defined at the point where:

$$\left(\frac{\partial u}{\partial y}\right)\Big|_{y=0} = 0 \qquad \ldots(15)$$

By considering Equations (14) and (15), it results that at the laminar separation point the second derivative of the pressure must also be zero. Immediately downstream from this point, the boundary layer may reattach itself, forming a turbulent boundary layer, or it may remain detached, creating a highly unsteady shear layer. The 'transition zone' is the region situated between the detachment point of the laminar boundary layer and its reattachment point as a turbulent one.

Further details, demonstrations and comparisons on this method are presented in Popov and Botez[52]. Other active control methods for the transition detection on a morphing wing are given[53,54].

Based on the above formulations, an approximation of the transition position can be computed from the pressure data. This method was successfully applied to the experimental pressure data collected during the Price-Païdoussis wind-tunnel tests to determine the transition point on the upper surface of the two rigid models. The comparison of the numerical transition prediction versus experimental transition estimated using the second derivative method on the pressure distribution was presented in Figs 10, 11 and 12. The second derivative method was applied on the raw experimental pressure data without the use of spline interpolations.

The derivative from the pressure distribution was calculated by using the second derivative as shown in Equation (16):

$$\left.\begin{aligned} \frac{\partial^2 p}{\partial x^2} &= \frac{\partial}{\partial x}\left(\frac{\partial p}{\partial x}\Big|_{iR}\right)\Big|_{iL} \\ \frac{\partial p}{\partial x}\Big|_{iR} &= \frac{p_{i+1}-p_i}{x_{i+1}-x_i} \end{aligned}\right| \Rightarrow \frac{\partial^2 p}{\partial x^2}$$
$$= \frac{p_{i+1}\cdot(x_i - x_{i-1}) - 2\cdot p_i \cdot (x_{i+1}-x_{i-1}) + p_{i-1}\cdot(x_{i+1}-x_i)}{(x_{i+1}-x_i)\cdot(x_i-x_{i-1})^2} \qquad \ldots(16)$$

This formulation was chosen because of the non-uniformity of the steps between two consecutive pressure taps. For the XFoil pressure distribution, the classic second derivative approximation, expressed by Equation (17), and obtained from the Taylor series, was used:

$$\frac{\partial^2 p}{\partial x^2} = \frac{p_{i+1} - 2\cdot p_i + p_{i-1}}{\Delta x^2} \qquad \ldots(17)$$

Case 2 - Analysis and testing for Mach number = 0.08 and angle-of-attack $\alpha = -1°$
Case 8 - Analysis and testing for Mach number = 0.09 and angle-of-attack $\alpha = 0°$
Case 15 - Analysis and testing for Mach number = 0.1 and angle-of-attack $\alpha = 2°$

Numerically, XFoil gives a single point for the transition, experimentally it is impossible to extract a discreet value for the transition on the upper surface; normally, there is a transition region for which an average can be calculated with an uncertainty value. Thus, the results

https://doi.org/10.1017/aer.2016.30 Published online by Cambridge University Press

Table 5
Transition results for numerical and experimental pressure data – original wing model

Angle-of-Attack(°)	Mach	Numerical Original				
(%c)	Experiment Original_min					
(%c)	Experiment Original_average					
(%c)	Experiment Original_max					
(%c)	+/− Experimental Uncertainty(% c)					
−1	0.08	34.50	33.00	36.50	40.00	3.50
0	0.09	31.13	31.00	32.50	34.00	1.50
2	0.1	27.58	20.00	27.00	34.00	7.00

Table 6
Transition results for numerical and experimental pressure data – optimised wing model

Angle-of-Attack(°)	Mach	Numerical Optimised (%c)	Experiment Optimised_min (%c)	Experiment Optimised_average (%c)	Experiment Optimised_max (%c)	+/− Experimental Uncertainty (%c)
−1	0.08	54.70	55.00	60.00	65.00	5.00
0	0.09	37.01	30.00	35.00	40.00	5.00
2	0.1	29.78	23.00	29.00	35.00	6.00

were presented in terms of the most probable minimum, maximum and average transition and the numerical prediction. Given that the speed interval is small, the transition interval variation from one speed to another at the same angle-of-attack is also small. This means that the pressure sensors show the transition is approximately in the same area for cases at the same angles of attack and small variation of the speed. This does not apply if the speed variation is high.

For the original wing model, Figs. 10(b)-12(b) show the comparison of the variation of the second derivative of pressure for experimental and numerically calculated data.

Table 5 presents the interval of the experimental transition and the numerical prediction for the cases presented in Figs 10-12(b). The transitions were presented in percentage of chord.

The uncertainty values were determined manually for each case, based on the pressure measurements, and were calculated as half the distance between the transition point's maximum and minimum possible locations.

Table 6 presents the interval of the experimental transition and the numerical prediction for the cases presented in Figs 10-12(a), which are for the optimised rigid wing model.

https://doi.org/10.1017/aer.2016.30 Published online by Cambridge University Press

Table 7(a)
Numerical transition results for all wind-tunnel cases

Angle-of-Attack	Mach	Original (%c)	Optimised (%c)	Numerical improvement (Original – Optimised in %c)
−2	0.08	37.82	57.75	19.93
	0.09	36.62	57.10	20.48
	0.1	35.73	56.47	20.74
−1	0.08	34.50	54.70	20.20
	0.09	33.34	53.67	20.33
	0.1	32.75	52.43	19.68
0	0.08	31.67	40.75	9.08
	0.09	31.13	37.01	5.88
	0.1	30.64	35.17	4.53
1	0.08	29.91	33.22	3.31
	0.09	29.44	32.43	2.99
	0.1	28.99	31.73	2.74
2	0.08	28.34	30.82	2.48
	0.09	27.93	30.27	2.34
	0.1	27.58	29.78	2.20

For the cases presented above, on average, the error between the numerical and experimental transition is between 0.5 and 2% for the original wing model and between 0.7 and 5% for the optimised wing model. However, the error can drop to less than 0.5% or go as high as 10% if the uncertainty interval is taken into account. The large interval in the experimental transition, especially in the case of the optimised wing model, is partially given by the position of the pressure sensors. In Section 5, it was mentioned that a different step was used when installing the pressure taps on the original and optimised wings. These results show that the original wing model, on which the sensors were installed using a variable step based on the numerical transition predictions, the uncertainty interval is much smaller than for the optimised wing on which the sensors were installed at a constant step. The previous observation confirms the attention that needs to be taken when installing the pressure sensors. An analysis of the number and positions of the sensors should be done, while taking into account numerical predictions, before tests are done in wind tunnel.

The differences between numerical and experimental transition were also dues to other factors, the precision of the aerodynamic solver XFoil, an insufficient number of sensors in regions where transition is expected to appear, the manner in which the experimental data was interpolated, human error. By improving any of the above differences, the error between the experimental readings and the theoretic prediction should decrease.

The results presented in Figs 10-12 show that using a reasonable number of sensors installed on the upper surface, and even in the absence of an interpolation method for the pressure data, preliminary results were obtained for the transition onset without the need of more complex measurement systems. The following Tables 7(a)-7(d), present the numerical and

https://doi.org/10.1017/aer.2016.30 Published online by Cambridge University Press

Table 7(b)
Estimated experimental transition results with uncertainty for all wind-tunnel cases for the original wing model

Angle-of-Attack	Mach	Experiment Original_min (%c)	Experiment Original_average (%c)	Experiment Original_max (%c)	+/− Uncertainty (%)
−2	0.08	40.00	45.00	50.00	5.00
	0.09	35.00	38.50	42.00	3.50
	0.1	35.00	37.50	40.00	2.50
−1	0.08	33.00	36.50	40.00	3.50
	0.09	33.00	35.00	37.00	2.00
	0.1	31.00	33.50	36.00	2.50
0	0.08	31.00	33.00	35.00	2.00
	0.09	31.00	32.50	34.00	1.50
	0.1	27.00	31.00	35.00	4.00
1	0.08	29.00	30.50	32.00	1.50
	0.09	28.00	30.00	32.00	2.00
	0.1	26.00	29.00	32.00	3.00
2	0.08	23.00	28.00	33.00	5.00
	0.09	23.00	28.00	33.00	5.00
	0.1	20.00	27.00	34.00	7.00

Table 7(c)
Estimated experimental transition results with uncertainty for all wind-tunnel cases for the optimised wing model

Angle-of-Attack	Mach	Experiment Original_min (%c)	Experiment Original_average (%c)	Experiment Original_max (%c)	+/− Uncertainty (%)
−2	0.08	55.00	61.00	67.00	6.00
	0.09	55.00	61.00	67.00	6.00
	0.1	55.00	60.00	65.00	5.00
−1	0.08	55.00	60.00	65.00	5.00
	0.09	50.00	55.00	60.00	5.00
	0.1	50.00	55.00	60.00	5.00
0	0.08	30.00	35.00	40.00	5.00
	0.09	30.00	35.00	40.00	5.00
	0.1	30.00	35.00	40.00	5.00
1	0.08	No estimation	No estimation	No estimation	No estimation
	0.09	30.0	35.00	40.00	5.00
	0.1	30.00	35.00	40.00	5.00
2	0.08	23.00	29.50	36.00	6.50
	0.09	23.00	28.50	34.00	5.50
	0.1	23.00	29.00	35.00	6.00

https://doi.org/10.1017/aer.2016.30 Published online by Cambridge University Press

Table 7(d)
Estimated experimental vs. numerical transition improvement for all wind-tunnel cases

Angle-of-Attack	Mach	Numerical improvement (%c)	Experimental improvement (%c)
−2	0.08	19.93	16.00
	0.09	20.48	22.50
	0.1	20.74	22.50
−1	0.08	20.20	23.50
	0.09	20.33	20.00
	0.1	19.68	21.50
0	0.08	9.08	2.00
	0.09	5.88	2.50
	0.1	4.53	4.00
1	0.08	3.31	No estimation
	0.09	2.99	5.00
	0.1	2.74	6.00
2	0.08	2.48	1.50
	0.09	2.34	0.50
	0.1	2.20	2.00

the experimental transition results for all the cases tested in the wind tunnel for the two wing models and the transition improvement obtained both numerically and experimental.

The Reynolds numbers range from 430 000 for Mach number 0.08 to 540 000 for Mach 0.1.

The improvements presented in Table 7(d) columns 3 and 4 were calculated using the following formula:

$$\text{improvement} = \left(\text{Transition}_{\text{morphed\_wing}} - \text{Transition}_{\text{original\_wing}}\right) 100 \quad \ldots (18)$$

Figures 13-15 present, for each speed, the comparison between the predicted and the estimated improvement.

As seen in Tables 7(a)-7(d) and in Figs 13-15, the experimental data showed greater improvement of the transition position than the numerical predictions for some of the cases, while for others it obtains similar results. The exceptions were at angle-of-attack 2° where the improvement percentage was smaller than what was numerically predicted.

Figure 16 represents the Lift versus Drag coefficient curve comparison between original and optimised wing models. It is evident that at Mach 0.08 the optimised shape is particularly performing, also that in all cases there is a marked reduction in the drag coefficient. Numerically, the drag reduction varies between 3% and 10% between original and optimised shape, with higher reductions at negative angles of attack.

Finally, for a better understanding of the optimisation results, both numerical and experimental, the performances of the original aerofoil were compared with the performances of the optimised shape (obtained from the optimisation at a single flight case, Mach number 0.1 and angle-of-attack 0°). The purpose of this comparison was to show that

https://doi.org/10.1017/aer.2016.30 Published online by Cambridge University Press

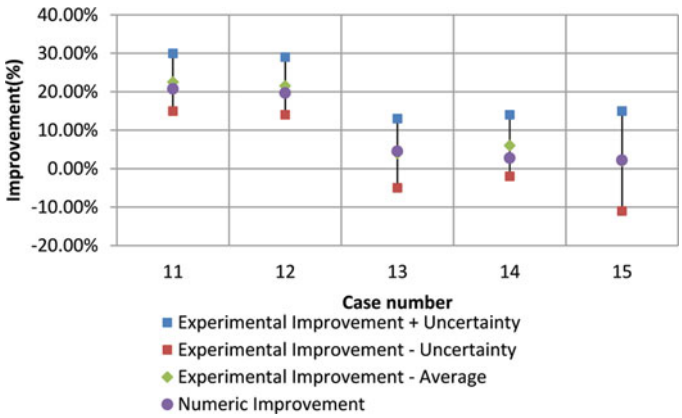

Figure 13. (Colour online) Transition improvement numerical vs. experimental with uncertainty margins for cases at Mach number = 0.1.

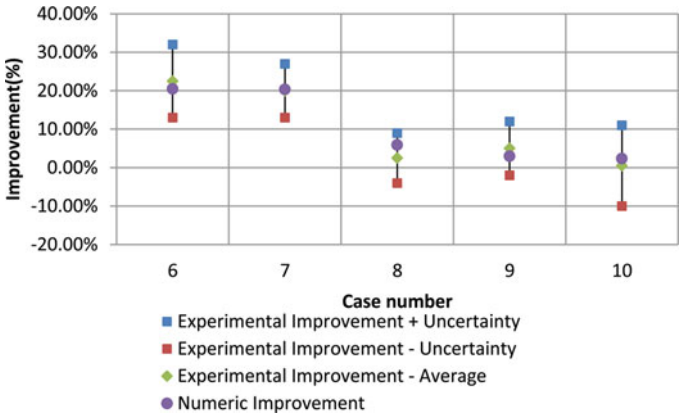

Figure 14. (Colour online) Transition improvement numerical vs. experimental with uncertainty margins for cases at Mach number = 0.09.

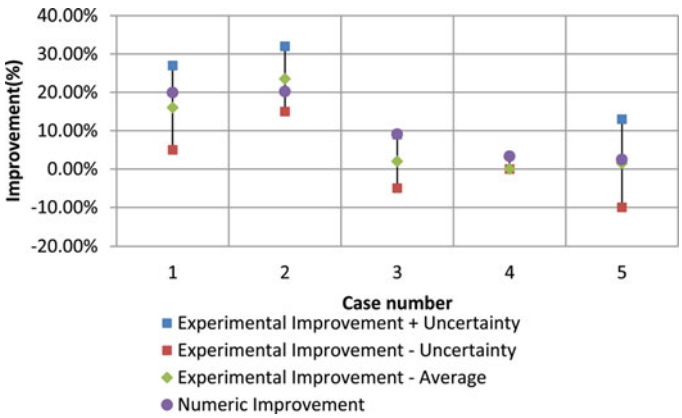

Figure 15. (Colour online) Transition improvement numerical vs. experimental with uncertainty margins for cases at Mach number = 0.08.

https://doi.org/10.1017/aer.2016.30 Published online by Cambridge University Press

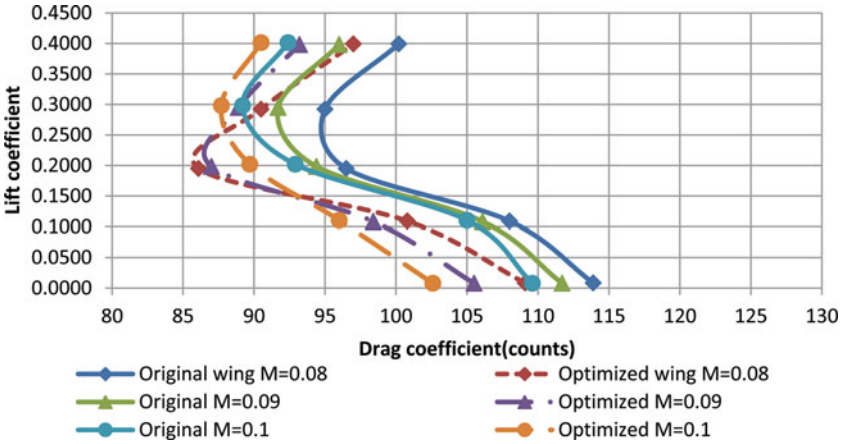

Figure 16. (Colour online) Comparison of the numerical drag coefficient (counts, one count $= 10^{-4}$) between original and optimised wing.

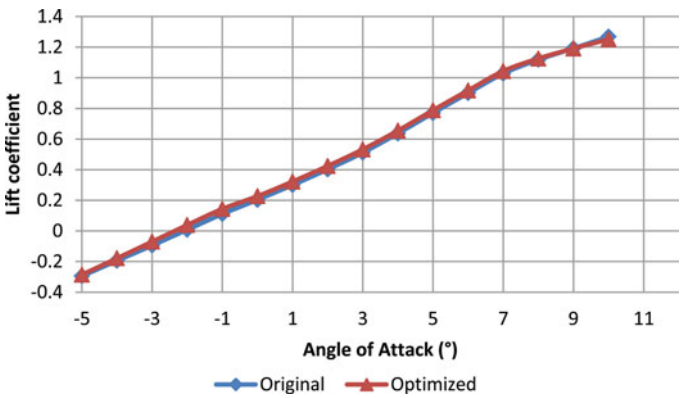

Figure 17. (Colour online) Lift coefficient curve comparison between original and optimised wing models for a large range of angles of attack and Mach number 0.1.

the optimised shape, although very efficient outside its optimisation condition, was not sufficiently performing in order to replace the original aerofoil; and that based on the observed performances of the optimised aerofoil, other optimal shapes should be researched to improve the original aerofoil for as many flight conditions as possible.

It can be seen in Fig. 17 that the lift coefficient is not affected by the new optimised shape, since the objective was concentrated on the drag and transition and curvature of the aerofoil was not modified.

Figure 18 presents the Lift-to-Drag curve and Fig. 19 presents the Transition-to-Drag curves for both original and optimised aerofoils. Both figures were drawn for a range of angles of attack between $-5°$ and $10°$. It was observed that the optimised aerofoil has improvements outside the design range at negative angles of attack up to $-3°$ and small improvements at $2°$ and $3°$ angles of attack. Above and below these thresholds the optimised shape differs in no way from the original aerofoil performances, with the exception of the negative ($-4°$ and $-5°$) and very high positive angles of attack ($9°$ and $10°$).

https://doi.org/10.1017/aer.2016.30 Published online by Cambridge University Press

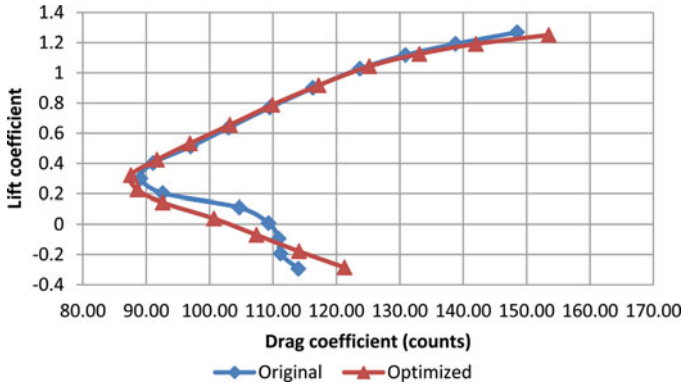

Figure 18. (Colour online) Lift-Drag curve comparisons between original and optimised wing models for a large range of angles of attack and Mach number 0.1.

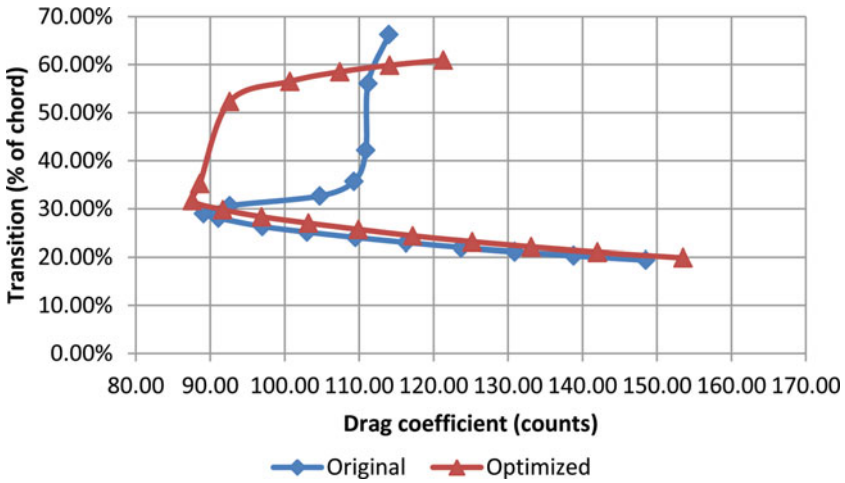

Figure 19. (Colour online) Transition-Drag curve comparisons between original and optimised wing models for a large range of angles of attack (−5° to 10°) and Mach number 0.1.

These results confirmed that the shape obtained with the genetic algorithm optimisation software for Mach number of 0.1 and angle-of-attack of 0° can be successfully used as an optimal shape for speeds and angles of attack situated in the immediate vicinity of the speed and angle-of-attack at which the optimisation took place. This aspect could be particularly useful when successive manoeuvres are done in a short period at small variations of speed and angle-of-attack values (as, for example, in the presented cases where the speeds vary between 20 m/s and 34 m/s). In these cases, it is sufficient to use a single optimal shape and to morph the wing to another optimal shape when the range of speeds or angles of attack increases beyond a problem-dependent value.

In this case, the optimised aerofoil has obtained improvements for both the angle-of-attack and speed variation. It is evident from the results presented above, that for the higher angles of attack (more than 1°) the original ATR 42 aerofoil should be optimised for each flight case

https://doi.org/10.1017/aer.2016.30 Published online by Cambridge University Press

instead of grouping them in order to maximise the chances of having a high improvement of the transition region and by consequence of the drag coefficient for all flight cases.

7.0 CONCLUSIONS

In the present paper, the first phase of a multi-disciplinary project for the development of a reduced scale morphing wing was presented. This first phase concerned the development, testing and validation of an optimisation genetic algorithm coupled with the XFoil aerodynamic solver, the development of a composite material and manufacturing of two rigid wing models for wind-tunnel testing. The objectives of the paper were to validate, over a range of angles of attack and speeds, the optimised shape of the ATR42 aerofoil for Mach 0.1 angle-of-attack 0°, to validate the composite material choice for these models in the wind tunnel, to analyse the relationship between the pressure sensors positions and numbers and the accuracy of the readings, and to validate a method for estimating the transition improvement from the pressure data collected during these tests.

The results, presented in Section 6.1, have shown that from an aerodynamic point of view an agreement was obtained between the numerical pressure distribution and the pressure distribution measured in the wind tunnel. On the lower surface of the models the agreement was not as good as on the upper surface due to the loss of one of the pressure taps and to the low number of sensors installed. Figures 7(c)-9(c), which presented a comparison between the pressure distribution for the original shape and the pressure distribution of the optimised shape, demonstrated that the pressure distribution was visibly affected by the skin's small vertical displacements, as the ones used for the optimised shape (less than 3 mm).

The results presented in Section 6.2 showed the estimation of the transition from experimental data using the second derivative of the pressure coefficient and its comparison with the numerically estimated transition. The results showed that the efficiency of the method depends on the number of sensors on the upper surface and on the step with which they were installed. Better results in the estimation of the transition were obtained for the original shape wing model where the step was varied as function of the numerical prediction (of the transition) compared with the estimations for the optimised shape model for which a constant step was used. These results have shown that more care should be taken when determining the number and positions of the sensors for a wind-tunnel model.

Regardless of these shortcomings, the method was useful for preliminary estimation of the transition region within a certain degree of accuracy, especially when no complex methods and tools are available, where the estimation time is an important variable or the collected data consists to pressure measurements.

The results presented in Tables 7(a)-7(d) validated the second derivative estimation method of the experimental transition and the optimisation of the aerofoil shape used for the optimised wing model. For almost all cases, a significant transition improvement was obtained. The average transition improvement was estimated to be at more than 10% of the chord with the maximum achieved being 20% of the chord. The numerically predicted improvement of the drag coefficient was also indirectly validated and the reductions were predicted to be up to 10% of the original values, with the average reduction of the drag coefficient being approximately 3% to 5%.

The present paper brings a multidisciplinary perspective on the upper surface morphing technique by applying it to a different aerofoil, using an in-house developed genetic algorithm, different from the algorithm that was used in the previous CRIAQ 7.1 project.

https://doi.org/10.1017/aer.2016.30 Published online by Cambridge University Press

The optimisation technique was validated with experimental testing in the Price-Païdoussis wind tunnel on two rigid wing model with the aim to apply it on an active morphing wing in the second phase of the project. In addition, this paper validates a method for determining the transition region on the upper surface from experimental pressure data and discusses the importance of the pressure sensors positions and numbers for obtaining accurate readings and results. A composite material was optimised, used for the complete manufacturing of each of the wing models and, was validated through wind-tunnel testing.

ACKNOWLEDGEMENTS

We would like to thank Professors Stuart Price and Michael Païdoussis from McGill University for the donation of their blow down subsonic wind tunnel, and Mr. Oscar Carranza and Master's student Manuel Flores Salinas for their dedicated work related to its functioning at the LARCASE laboratory at ETS. We would also like to indicate our appreciation of the work on the composite wing model conducted by Professor Simon Joncas, Master student François Michaud and internship student Robin Calestreme. Thanks are due to the Natural Sciences and Engineering Research Council NSERC for the funds received in the frame of the Canada Research Chair in Aircraft Modeling and Simulation.

REFERENCES

1. PATRON FELIX, S.R., KESSACI, A. and BOTEZ, R.M. Horizontal flight trajectories optimization for commercial aircraft through a flight management system, *The Aeronautical j*, 2013, **118**, (1210), p 201.
2. PATRON FELIX, S.R. and BOTEZ, R.M. New altitude optimization algorithm for the flight management system CMA-9000 improvement on the A310 and L-1011 aircraft, *Aeronautical J*, 2013, **177**, (1194), pp 787-805.
3. PECORA, R., BARBARINO, S., CONCILIO, A., LECCE, L. and RUSSO, S. Design and functional test of a morphing high-lift device for a regional aircraft, *J Intelligent Material Systems and Structures*, 2011, **22**, (10), pp 1005-1023.
4. DIODATI, G., CONCILIO, A., RICCI, S., DE GASPARI, A., LIAUZUN, C. and GODARD, J.L. Estimated performance of an adaptive trailing-edge device aimed at reducing fuel consumption on a medium-size aircraft, 8690-14, Smart Structures/NDE Conference, 10-14 March 2013, San Diego, California, US.
5. PECORA, R., AMOROSO, F. and LECCE, L. Effectiveness of wing twist morphing in roll control, *J Aircr*, 2012, **49**, (6), pp 1666-1674.
6. GAMBOA, P., VALE, J., LAU, F. and SULEMAN, A. Optimization of a morphing wing based on coupled aerodynamic and structural constraints, *AIAA J*, 2009, **47**, (9), pp 2087-2104.
7. FALCÃO, L., GOMES, A.A. and SULEMAN, A. Aero-structural design optimization of a morphing wingtip, *J Intelligent Material Systems and Structures*, 2011, **22**, (10), pp 1113-1124.
8. SUGAR GABOR, O., KOREANSCHI, A. and BOTEZ, R.M. Optimization of an unmanned aerial systems' wing using a flexible skin morphing wing, *SAE Int J Aerospace*, 2013, **6**, (1), pp 115-121.
9. SUGAR GABOR, O., SIMON, A., KOREANSCHI, A. and BOTEZ, R.M. Application of a morphing wing technology on hydra technologies unmanned aerial system UAS-S4, ASME International Mechanical Engineering Congress and Exposition IMECE14, 14-20 November 2014, Montreal, Canada.
10. SOFLA, A.Y.N., MEGUID, S.A., TAN, K.T. and YEO, W.K. Shape morphing of aircraft wing: Status and challenge, *Elsevier J, Material and Design*, 2010, **31**, (3), pp 1284-1292.
11. VASISTA, S., TONG, L. and WONG, K.C. Realizations of morphing wings: A multidisciplinary challenge, *J Aircr*, 2012, **49**, (1), pp 11-28.
12. EPPLER, R. *Airfoil Design and Data*, 1990, Edition Springer-Verlag, Berlin-Heidelberg GmbH, pp 163-510, ISBN is 978-3-662-02648-9.

https://doi.org/10.1017/aer.2016.30 Published online by Cambridge University Press

13. MULLER, T.J. (Ed). Low Reynolds Number Aerodynamics, Proceedings of the Conference Notre-Dame, 5-7 June 1989, Indiana, US.
14. POPOV, A.V., BOTEZ, R.M., MAMOU, M., MEBARKI, Y., JAHRHAUS, B., KHALID, M. and GRIGORIE, T.L. Drag reduction by improving laminar flows past morphing configurations, AVT-168 NATO Symposium on the Morphing Vehicles, 20-23 April 2009, Evora, Portugal.
15. BOTEZ, R.M., MOLARET, P. and LAURENDEAU, E. Laminar flow control on a research wing project presentation covering a three year period, CASI Aircraft Design and Development Symposium, 25-26 April 2007, Toronto, Ontario, Canada.
16. GRIGORIE, L.T., POPOV, A.V., BOTEZ, R.M., MAMOU, M. and MÉBARKI, Y. A hybrid fuzzy logic proportional-integral-derivative and conventional on-off controller for morphing wing actuation using shape memory alloy Part 1: Morphing system mechanisms and controller architecture design, *Aeronautical J*, 2012, **116**, (1179), pp 433-449.
17. SAINMONT, C., PARASCHIVOIU, I., COUTU, D., BRAILOVSKI, V., LAURENDEAU, E., MAMOU, M., MEBARKI, Y. and KHALID, M. Boundary layer behaviour on a morphing airfoil: Simulation and wind tunnel tests, CASI AERO'09 Conference Aerodynamics Symposium, 2009.
18. GRIGORIE, L.T., BOTEZ, R.M. and POPOV, A.V. Design and experimental validation of a control system for a morphing wing, AIAA Atmospheric Flight Mechanics Conference, Invited Session Paper, 13-17 August 2012, Minneapolis, Minnesota, US.
19. GRIGORIE, L.T., BOTEZ, R.M., POPOV, A.V., MAMOU, M. and MÉBARKI, Y. A new morphing mechanism for a wing using smart actuators controlled by a self-tuning fuzzy logic controller, AIAA Centennial of Naval Aviation Forum: 100 Years of Achievement and Progress, 20-22 September 2011, Virginia Beach, Virginia, US.
20. POPOV, A.V., BOTEZ, R.M., GRIGORIE, T. L., MAMOU, M. and MEBARKI, Y. Real time airfoil optimization of a morphing wing in wind tunnel, *AIAA J Aircr*, 2010, **47**, (4), pp 1346-1354.
21. POPOV, A.V., BOTEZ, R. M., GRIGORIE, T. L., MAMOU, M. and MEBARKI, Y. Closed loop control of a morphing wing in wind tunnel, *AIAA J Aircr*, 2010, **47**, (4), pp 1309-1317.
22. MITCHELL, M. *An Introduction to Genetic Algorithms*, 1996, Cambridge, Massachusetts, US, MIT Press.
23. COLEY, D.A. *An Introduction to Genetic Algorithms for Scientists and Engineers*, 1999, World Scientific Publishing, Singapore.
24. KULFAN, B.M. and BUSSOLETTI, J.E. Fundamental parametric geometry representations for aircraft component shapes, AIAA 2006–6948 Technical Paper, 2006.
25. DEB, R.A.K. Simulated binary crossover for continuous search space, *Complex Systems*, 1995, **9**, (3), pp 115-148.
26. DRELA, M. and YOUNGREN, D. XFOIL Version 6.96 Documentation, 2001, http://web.mit.edu/drela/Public/web/xfoil/xfoil_doc.txt.
27. DRELA, M. XFoil: An Analysis and Design System for Low Reynolds Number Airfoils, Low Reynolds Number Aerodynamics, Proceedings of the Conference Notre-Dame, 5-7 June 1989, Indiana, US.
28. DRELA, M. An integral boundary layer formulation for blunt trailing edges, AIAA 89-2200 Technical Paper, 1989.
29. DRELA, M. Implicit implementation of the full *En* transition criterion, Proceedings of 21st Applied Aerodynamics Conference, 23-26 June 2003, Orlando, Florida, US, AIAA 2003–4066.
30. VAN INGEN, J.L. The eN method for transition prediction. Historical review of work at TU Delft, AIAA 38th Fluid Dynamics Conference and Exhibit, 23-26 June 2008, Seattle, Washington, US, AIAA 2008–3830.
31. BEN MOSBAH, A., FLORES SALINAS, M., BOTEZ, R. and DAO, T. New methodology for wind tunnel calibration using neural networks - EGD approach, *SAE Int J Aerospace*, 2013, **6**, (2), pp 761-766, doi:10.4271/2013-01-2285.
32. BORLOW, J., RAE, W. and POPE, A. *Low Speed Wind Tunnel Testing*, 1999, Wiley, Hoboken, New Jersey, US.
33. MICHAUD, F., JONCAS, S. and BOTEZ, R.M. Design, manufacturing and testing of a small-scale composite morphing wing, 19th International Conference on Composite Materials, 28 July-2 August 2013, Montreal, Quebec, Canada.
34. CALESTREME, R. Conception et fabrication de modelés d'aile en composite a fin de les tester dans la soufflerie Price-Païdoussis, Master Project, École de Technologie Supérieure, 2012, Montreal, Quebec, Canada.

https://doi.org/10.1017/aer.2016.30 Published online by Cambridge University Press

35. STORMS, B., TAKAHASHI, T.T. and ROSS, J.C. Aerodynamic influence of a finite-span flap on a Simpla wing, SAE Technical paper 951977, 1995.
36. BASTEDO, W.G. and MUELLER, T.J. Spanwise variation of laminar separation bubbles on wings at low Reynolds numbers, *J Aircr*, 1986, **23**, (9), pp 687-694.
37. Aerolab. Data Acquisition Systems. Available at: http://www.aerolab.com/products/data-acquisition-systems/, accessed in February 2015.
38. SHAW, R. The influence of hole dimensions on static pressure measurements, *J Fluid Mechanics*, 1960, **7**, (4), pp 550-564.
39. TAVOULARIS, S. *Measurement in Fluid Mechanics*, 2005, Cambridge University Press, New York, US.
40. VERCAUTEREN, J., BOSSCHAERTS, W., BAELMANS, M. and PERSOONS, T. Numerical investigation on the measurement error of static pressure taps in small scale channels. *Proceedings Power MEMS, Proceedings of the 10th International Workshop on Micro and Nanotechnology for Power Generation and Energy Conversion Applications (PowerMEMS)*, December 1-3 2010, Leuven, Belgium, pp 295-298.
41. REYNOLDS, O. An experimental investigation of the circumstances which determine whether the motion of water shall be direct or sinuous, and of the law of resistance in parallel channels, *Philosophical Transactions of the Royal Society*, London, 1883, **174**, pp 935-982.
42. SCHLICHTING, H. and GERSTEN, K. *Boundary-Layer Theory*, 2000, Springer-Verlag, Berlin, pp 377-378.
43. MENTER, F.R., LANGTRY, R.B., LIKKI, S.R., SUZEN, Y.B., HUANG, P.G. and VÖLKER, S. A correlation-based transition model using local variables – part I: model formulation. *Journal of turbomachinery*, 2006, **128**, (3), pp 413-422.
44. SILISTEANU, P.D. and BOTEZ, R.M. Transition-flow-occurrence estimation: A new method, *J Aircr*, 2010, **47**, (2), pp 703-708.
45. GRANVILLE, P.S. The calculation of the viscous drag of bodies of revolution, *David Taylor Model Basin Report* 1953, p 849.
46. MICHEL, R. Étude de la transition sur les profils d'aile; Établissement d'un critére de determination du point de transition et calcul de la trainée de profil en incompressible, ONERA Report 1/1578, 1952.
47. WAZZAN, A.R., GAZLEY, C. and SMITH, A.M.O. Tollmien-schlichting waves and transition, *Progress in Aerospace Sciences*, 1979, **18**, (2), pp 351-392.
48. MAMOU, M., YUAN, W. and KHALID, M. Transition prediction in low reynolds airfoil flows using finite element/difference solvers coupled with the en method: A comparative study, AIAA Paper 2006–3176, 2006.
49. KHRABROV, A. and OI, M.V. Effects of flow separation on aerodynamic loads in linearized thin airfoil theory, *J Aircr*, 2004, **41**, (4), pp 944-948.
50. MENTER, F.R., LANGTRY, R.B., LIKKI, S.R., SUZEN, Y.B., HUANG, P.G. and VOLKER, S. A correlation-based transition model using local variables – part I: Model formulation, *J Turbomachinery*, 2006, **128**, pp 413-422.
51. LANGTRY, R.B., MENTER, F.R., LIKKI, S.R., SUZEN, Y.B., HUANG, P.G. and VOLKER, S. A correlation-based transition model using local variables – part II: Test cases and industrial applications, *J Turbomachinery*, 2006, **128**, pp 423-434.
52. POPOV, A.V., BOTEZ, R.M. and LABIB, M. Transition point detection from the surface pressure distribution for controller design, *J Aircr*, 2008, **45**, (1), pp 23-28.
53. GRIGORIE, T.L. and BOTEZ, R.M. New adaptive controller method for SMA hysteresis modelling of a morphing wing, *Aeronautical J*, 2010, **114**, (1151), pp 1-13.
54. GRIGORIE, L.T., POPOV, A.V., BOTEZ, R.M., MAMOU, M. and MÉBARKI, Y. A hybrid fuzzy logic proportional integral-derivative and conventional on-off controller for morphing wing actuation using shape memory alloy, part 2: Controller implementation and validation, *Aeronautical J*, 2012, **116**, (1179), pp 451-465.

https://doi.org/10.1017/aer.2016.30 Published online by Cambridge University Press